

# Accepted Manuscript

Tidal energy extraction in three-dimensional ocean models

Alice J. Goward Brown, Simon P. Neill, Matthew J. Lewis

PII: S0960-1481(17)30339-7

DOI: [10.1016/j.renene.2017.04.032](https://doi.org/10.1016/j.renene.2017.04.032)

Reference: RENE 8727

To appear in: *Renewable Energy*

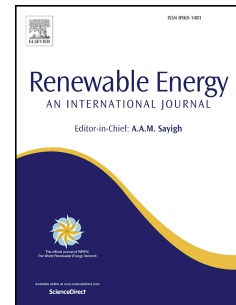
Received Date: 6 October 2016

Revised Date: 11 April 2017

Accepted Date: 14 April 2017

Please cite this article as: Goward Brown AJ, Neill SP, Lewis MJ, Tidal energy extraction in three-dimensional ocean models, *Renewable Energy* (2017), doi: 10.1016/j.renene.2017.04.032.

This is a PDF file of an unedited manuscript that has been accepted for publication. As a service to our customers we are providing this early version of the manuscript. The manuscript will undergo copyediting, typesetting, and review of the resulting proof before it is published in its final form. Please note that during the production process errors may be discovered which could affect the content, and all legal disclaimers that apply to the journal pertain.



# Tidal energy extraction in three-dimensional ocean models

Alice J. Goward Brown

Simon P. Neill

Matthew J. Lewis

*School of Ocean Sciences, Menai Bridge, Bangor, Gwynedd, LL59 5AB*

---

## Abstract

Access to high performance computing has made 3-D modelling de rigueur for tidal energy resource assessments. Advances in computing resources and numerical model codes have enabled high resolution 3-D ocean models to be applied at basin scales, albeit at a much higher computational cost than the traditional 2-D modelling approach. Here, a comparison between 2-D and 3-D tidal energy extraction modelling techniques is undertaken within a 3-D modelling framework, and differences between the methods are examined from both resource and impact assessment perspectives. Through a series of numerical experiments using the Regional Ocean Modeling System (ROMS), it is shown that 3-D tidal energy extraction can be successfully incorporated in a regional ocean model of the Pentland Firth - one of the top regions in the world for tidal stream energy development. We demonstrate that resolving 3-D flow is important for reducing uncertainty in environmental resource assessments. Further, our results show that 2-D tidal energy extraction methods lead to a misrepresentation of the velocity profile when applied to 3-D models, demonstrating the importance of resolving 3-D flows in the vicinity of tidal arrays.

*Keywords:* Tidal energy resource, Tidal energy modelling, Tidal power,

24 3-D tidal model, ROMS, Pentland Firth

---

## 25 **1. Introduction**

26 When identifying a tidal energy site, the water depth, proximity to a grid  
 27 connection and an energetic resource (peak spring tidal flows in excess of  
 28 2m/s) are the main characteristics considered (Couch and Bryden, 2006;  
 29 Bryden and Melville, 2004). Tidal currents are three-dimensional, and  
 30 contain non-linear features (i.e turbulence, eddy fields and overtides),  
 31 hence, in order to properly characterise the available resource, hub-height  
 32 velocities should be used for characterisation of inflow conditions (Polagye  
 33 et al., 2010). In tidal stream energy applications, current speed information  
 34 is required to predict the forces on the turbine and power output. In first  
 35 generation tidal stream, shallow water ( $< 100\text{m}$ ) environments, the fastest  
 36 tidal currents are found between the middle and surface of the water  
 37 column (Prandle, 1982), subsequently tidal stream turbines are designed to  
 38 extract the flow in the upper reaches of the water column (Blunden and  
 39 Bahaj, 2007). Modelling tidal energy extraction poses a multi-scale  
 40 challenge to the tidal energy research community (Adcock et al., 2015),  
 41 turbine scale - the hydrodynamic flow between individual devices and array  
 42 scale - the interaction of the tidal stream hydrodynamics with the entire  
 43 array, where the research question posed ultimately dictates the suitability  
 44 of the methods used. Traditionally, three-dimensional (3-D) Computational  
 45 Fluid Dynamics (CFD) models have been employed to study individual  
 46 turbines, whereas two-dimensional (2-D) modelling techniques have been  
 47 used for large array scale modelling, with turbines represented using the

48 actuator disc concept applied as an area of enhanced drag stress within a  
 49 regional model (Robins et al., 2014; Draper et al., 2010; Ahmadian et al.,  
 50 2012; Oldfield and Borthwick, 2010). More recently, researchers have begun  
 51 using 3-D models to assess the theoretical resource of regions (Lewis et al.,  
 52 2015; Neill et al., 2014) and assess the potential impacts of tidal energy  
 53 extraction (Neill et al., 2012). Computational advancements have made  
 54 tidal energy extraction feasible within regional 3-D models. For accurate  
 55 resource assessments, it is necessary to include the interaction of the tidal  
 56 stream with the tidal array (Bryden et al., 2007), since the extraction of  
 57 tidal energy will lead to changes within the velocity structure (Neill et al.,  
 58 2012; Yang et al., 2013). The use of depth-averaged velocities is therefore  
 59 inaccurate for resource assessments because the velocity profile in a realistic  
 60 case will be distorted, such that the velocities across the swept area of the  
 61 rotor will be less than those above and below the device. Accurately  
 62 defining the flow around the turbine will reduce uncertainty in resource  
 63 calculations. The increase in turbulence and the velocity deficit caused by  
 64 upstream turbines will impact the turbine yield downstream. Turbine wake  
 65 comparisons between flume experiments and CFD actuator disc models  
 66 show similar characteristics (Harrison et al., 2010). It is hypothesised that  
 67 flow bypass around the turbine will change the projected resource from that  
 68 calculated by a depth-averaged model.

### 69 *1.1. Impact Assessments*

70 Environmental impact assessments have identified a number of key physical  
 71 and biological parameters which could be affected by feedbacks between  
 72 in-stream tidal energy extraction and the local hydrodynamics. Namely:

73 flow hydrodynamics, sediment dynamics, artificial reef effects and habitat  
74 disruption caused by the installation, operation and maintenance of devices  
75 (Shields et al., 2011; Shapiro, 2011), the impacts of which have yet to be  
76 successfully quantified. In the region of the array, 2-D extraction methods  
77 will reduce velocities over the whole water column. In reality the tidal  
78 current will increase around the tidal stream device (Bahaj et al., 2007;  
79 Myers and Bahaj, 2005), which is reproducible using a 3-D method (Roc  
80 et al., 2013). Research by Vogel et al. (2013), identifies that in order to  
81 match the total power removed by a 2-D array to that removed by a 3-D  
82 array, the 2-D model requires a lower thrust to be applied to the flow than  
83 the 3-D simulation, which would lead to a higher flow speed through the  
84 array. Additionally, previous methods where an enhanced bed friction is  
85 used to represent tidal stream turbines in a 3-D model will ultimately  
86 misrepresent the vertical flow bypass around the device (i.e Neill et al.  
87 (2012), Figure 1). With the 2-D method there will be a higher bottom drag  
88 associated with the region of the array, which will have consequences for  
89 sediment transport applications.

90 The aim of this research is to use a three dimensional (3D) hydrodynamic  
91 model to quantify the differences between using depth-averaged and 3-D  
92 numerical methods for tidal energy extraction, in order to help reduce  
93 uncertainty within resource and environmental impact assessments and to  
94 highlight when a 3-D resource assessment is required. Tidal stream  
95 extraction is included in the numerical model using a methodology based  
96 on that developed by Roc et al. (2013) which applies the actuator disc  
97 concept to the 3D Regional Ocean Modeling System (ROMS). The paper

98 applies both methods to an idealised model of an energetic tidal channel to  
 99 examine the reliability of depth-averaged tidal extraction methods when  
 100 water depth is increased between the upper and lower limits of first  
 101 generation tidal energy sites (Section 3). The methods are then applied to a  
 102 regional model of the Pentland Firth and the impact of each method on the  
 103 flow-field is explored from an environmental impact assessment perspective.  
 104 The Pentland Firth has a world-leading tidal stream resource and hence is  
 105 of great interest to UK tidal energy development (Murray and Gallego,  
 106 2017). The environmental impact focus will be on changes to flow behavior  
 107 with a view to future works on impacts to sediment dynamics. Sandbanks  
 108 are important coastal features which are valuable to the aggregate and  
 109 fishing industries and also naturally protect coastlines through the  
 110 dissipation of wave energy (Neill et al., 2012).

## 111 **2. Numerical Modelling**

112 This study used the Regional Ocean Modeling System (ROMS), to compare  
 113 tidal energy extraction methodologies. ROMS has been used in recent  
 114 publications of resource assessments (Thyng and Riley, 2010; Lewis et al.,  
 115 2015; Robins et al., 2015). However, these works have not considered the  
 116 variability of the tidal current resource over the water column. Tidal energy  
 117 extraction is parameterised within the ROMS source code using a method  
 118 developed by Roc et al. (2013), described in Section 2.2.

### 119 *2.1. ROMS*

120 ROMS (Regional Ocean Modeling System) is an open-source 3-D model  
 121 which solves the hydrostatic Navier-Stokes equations using a Boussinesq

approximation on a structured horizontal grid with terrain following sigma layers (Shchepetkin and McWilliams, 2005). ROMS undergoes continuous development by its active user community led by Rutgers University and the University of California, Los Angeles ([www.myroms.org](http://www.myroms.org)). It is suitable for a wide range of applications, over a variety of scales from idealised analytical studies (Thyng and Riley, 2010) to coastal and regional domains (Ohlmann and Mitarai, 2010), toolboxes have been created to couple ROMS with various models, such as the wave model SWAN and sediment sub-models (Warner et al., 2010).

## 2.2. Modelling tidal energy extraction

In this study, an external force ( $F_t$ ) is applied to the ROMS momentum equations to simulate the impact of tidal energy extraction (Equation 1) (Sánchez et al., 2014). The force of a turbine acting on the fluid ( $F_t$ ) is defined by Equation 2, where  $C_t$  is the dimensionless thrust coefficient, related to the porosity of the disc by the induction factor  $a$ .  $a$ , is a dimensionless quantity ranging between 0 and 1 which represents the reduction in flow velocity (Harrison et al., 2009).

In order to account for realistic flow conditions, it is more accurate to define  $F_t$  as a function of the flow velocity at the disk location ( $\vec{U}_d$ ) instead of the unconstrained upstream velocity ( $U_\infty$ ), in order for flow interaction with the turbine structure to be taken into account.

$$\begin{cases} \frac{\delta u}{\delta t} + \vec{v} \cdot \nabla u - fv = -\frac{\delta \phi}{\delta x} - \frac{\delta}{\delta z} \left( -K_M \frac{\delta u}{\delta z} - v \frac{\delta u}{\delta z} \right) + A_M \left( \frac{\delta^2 \bar{u}}{\delta x^2} + \frac{\delta^2 \bar{v}}{\delta y^2} \right) + \frac{1}{2} F_t \\ \frac{\delta v}{\delta t} + \vec{v} \cdot \nabla v + fu = -\frac{\delta \phi}{\delta y} - \frac{\delta}{\delta z} \left( -K_M \frac{\delta v}{\delta z} - v \frac{\delta v}{\delta z} \right) + A_M \left( \frac{\delta^2 \bar{v}}{\delta x^2} + \frac{\delta^2 \bar{u}}{\delta y^2} \right) + \frac{1}{2} F_t \end{cases} \quad (1)$$

$A_M$  represents the horizontal eddy viscosity,  $K_M$  the vertical viscosity,  $u, v$

are the velocity components in  $x$  and  $y$  respectively.  $z$  is the water depth,  $\vec{v}$  is the mean velocity vector and  $f$  is the coriolis parameter.  $\phi$  is the dynamic pressure which is equal to the total pressure,  $P$ , divided by the background density  $\rho_0$ .  $F_t$  is the force being applied over the turbine swept area ( $A_D$ ), characterised by the dimensionless thrust coefficient  $C_t$  (Equation 2).

$$C_t = \frac{F_t}{\frac{1}{2}\rho A_D U_\infty^2} = 4a(1-a) \quad (2)$$

Power extraction from the fluid (disregarding any mechanical losses) can be defined as the force multiplied by the rate of work done. According to the definition of the induction factor the extracted power can thus be described as:

$$Power = F_t \times U_d = 2\rho A_d U_\infty^3 a(1-a)^2 \quad (3)$$

For the 3-D extraction method, the force was applied over an area specified in x,y and z directions. A detailed methodology for the implementation of the turbines within the ROMS model can be found in Roc et al. (2013). The 2-D tidal extraction was implemented in the 3-D model by applying the force term over an area in which  $y$  was the water column depth and  $x$  was the width of the grid cell perpendicular to the dominant flow direction. In this case, the force term was adjusted accordingly to account for the increased area of tidal energy extraction. To ensure the amount of energy extracted by the turbine is equal for both cases the individual input and output velocities were compared (Table 1; Figure 2). The support structure is neglected in this instance in order to enable the method to be applicable to multiple turbine designs.



165 The key turbine operating parameters were assumed (Table 1; Myers and  
 166 Bahaj (2005)). This was not an attempt to represent a specific device,  
 167 however it was intended to represent a typical first-generation tidal stream  
 168 turbine.

### 169 **3. Application to an Idealised Channel**

170 An idealised channel model is created to compare the two methods within  
 171 an environment which is easily quantifiable. Initially a comparison is made  
 172 between the two methods to ensure that both methods are reducing the  
 173 depth-averaged velocities by the same amount, before comparing the  
 174 velocity profiles and establishing what impacts there might be on resource  
 175 and environmental impact assessments as a result of these differences  
 176 (Section 3.2). Finally, both methods are tested in models which become  
 177 progressively deeper. This final test determines the differing levels of  
 178 accuracy between the methods in increasingly more complex environments  
 179 (Section 4).

#### 180 *3.1. Model Setup*

181 A channel with dimensions similar to that of the Pentland Firth is  
 182 simulated (length of 30km, a width of 20km). Initially it has a constant  
 183 depth of 30m, the lower limit of first generation tidal stream sites. Grid  
 184 spacing ( $\delta x, \delta y$ ) was equal to 100m (the diameter of the turbine, plus 5  
 185 diameters of spacing either-side) and was 3m in the vertical to ensure the  
 186 area of the turbine was resolved by at-least 3 evenly-spaced sigma layers.  
 187 The lateral boundaries were closed and a free slip condition applied. A  
 188 constant inflow of 2m/s was imposed at the upstream channel boundary.

189 The downstream boundary was clamped for depth averaged velocities, and  
 190 a radiation condition was used for 3-D momentum. The free surface was  
 191 clamped to enable the comparison of the two methods without the  
 192 fluctuation of the free-surface. A drag coefficient of 0.0025, similar to other  
 193 studies of tidal channel (Baston et al., 2013), was imposed at the bed and  
 194 the model was run for 48 hours, long enough for the model to reach a  
 195 steady state (where velocities at the turbine location vary less than 1%  
 196 between each 10 second time-step).  
 197 The turbine array is rated at 0.6MW and has a rated velocity of 2.5m/s. It  
 198 is represented by a mid-depth force term (Equation 2). For 3-D tidal  
 199 extraction, the height of the turbine ( $T_D$ , equivalent to the turbine  
 200 diameter) is equal to 10m. For the 2-D extraction case  $T_D$  is equal to the  
 201 water depth (30m). The array of turbines is located in the middle of the  
 202 top third of the channel to enable the wake to freely develop; The blockage  
 203 ratio ( $B_R$ ), where  $B_R = \frac{A_D}{length_{x,y}}$ , of the turbine within the channel equates  
 204 to 5% in x and 3% in y. The area of the turbine,  $A_D$  is equal to  $\delta x, y \times T_D$   
 205 Adcock et al. (2015) recommends boundary lengths of 10 times those of the  
 206 turbine array. In order to ensure that the model boundaries were  
 207 sufficiently far from the turbine, multiple model runs were performed with  
 208 an increasing  $B_R$ . The velocities were extracted at the model boundary and  
 209 compared with a control (no turbine) case to ensure that perturbations  
 210 resulting from the turbine were not amplified by the boundaries.

### 211 3.2. Results : Velocity profile

212 Both the depth-averaged extraction and 3-D extraction reduce the  
 213 depth-averaged velocity field across the turbine area by 10%, from the

input velocity of 2m/s to 1.8m/s (Figure 2). The flow reduction across the 3-D disc is greater (Figure 3). This discrepancy, which in this case is of the order of 30cm/s, should be considered when making resource assessments. Wake effects from each method converge approximately 50 turbine diameters downstream of the region of energy extraction however a localised acceleration around the 3-D disc can be observed.

#### 4. Results: Idealised Tidal Energy Extraction in Deeper Water Environments

In this scenario, the depth within the idealised channel model is increased from 30m to 60m and 90m (in accordance with typical tidal-stream energy site classifications, Blunden and Bahaj (2007)). In each of these three cases, the height ( $T_D$ ) of the 3-D turbine is increased to maintain a blockage ratio in the vertical of 1/3 Whelan et al. (2009), and the thrust coefficient altered accordingly. The velocity for all cases remains a constant 2m/s, forced at the upstream channel boundary. For all cases, both the depth-averaged extraction and 3-D extraction reduce the depth-averaged velocity field from the input velocity of 2m/s to  $\sim 1.8$ m/s.

##### 4.1. Results : Power density

The amount of velocity reduction as a result of tidal energy extraction increases with water depth for the 3-D method, but decreases for the 2-D method (Table 2). The difference in velocity between the scenarios is between 2 and 5cm/s. The power density (Equation 4) is calculated for all cases (Figures 4 to 6), where Power ( $P$ ) divided by an area is equal to the kinetic energy ( $KE$ ) of the flow multiplied by the velocity ( $u$ ) within the

area specified. The results of Figures 4 to 6 is summarised in Table 2. It is observed that with the increase in channel depth, the difference between the maximum calculated power density in the channel increases. The difference in calculated power density for the two methods ranges from 1.7kW/m<sup>2</sup> for the original 30m channel depth case, to 2kW/m<sup>2</sup>. With the calculated power density for the 2-D case equal to 3298W/m<sup>2</sup> and 3405W/m<sup>2</sup> and for the 3-D case the calculated power density across the disc was equal to 1595W/m<sup>2</sup> and 1406W/m<sup>2</sup> for the channels with depths of 30m and 90m respectively.

$$P/A = KE \cdot u = \frac{1}{2}\rho u^3 \quad (4)$$

## 5. Case Study - Pentland Firth

The Pentland Firth, an approximately 20km long channel which separates the Isles of Orkney from the Scottish mainland, connects the North Atlantic Ocean with the North Sea. The tidal dynamics within the Pentland Firth and indeed the Orkney islands are notorious for their complex tidal dynamics and large tidal resource (Easton et al., 2012; Neill et al., 2014). The tides in the region are predominantly semi-diurnal; Despite its world leading tidal current speeds, the  $M_2$  amplitude of the vertical tide at the outer-reaches of the Pentland Firth is not remarkable, 1.02m at Wick (East) and 1.35m at Scrabster (West). Hence, it is the combination of the 2 hour phase difference between the North Atlantic end of the channel and the North Sea end of the channel (see Figure 7), and the complex geography resulting from the existence of many islands and

headlands, which serve to further augment the tidal currents, leading to peak spring current speeds which exceed 4m/s, making the Pentland Firth a world leading site for tidal energy development (Murray and Gallego, 2017). Four sites, with a total capacity of 800MW, have been leased by the crown estate for development by tidal energy companies (Figure 8 a), the largest of which is the *Inner Sound* site, a 400MW site which was leased to MeyGen for development in the last quarter of 2014 (Crown Estate, 2010; MeyGen, 2010). The Inner Sound of Stroma is a prominent island channel located between the Scottish mainland and the Isle of Stroma. Here peak spring currents exceed 3.5m/s. The capacity of the planned tidal energy development within the Inner Sound of Stroma is equal to that of the other three leased sites combined. Depths within the Pentland Firth range from maximum depths in exceedance of 80m in the main channel to depths of 30m in the Inner Sound which shoal gradually towards the coastline. The Carbon Trust (2011) predicts that the tidal resource of the Pentland Firth, accounting for constraints on the extraction of tidal energy (i.e: water depth, grid connections, shipping pathways and flow velocity), will make up 30% of the UK's practical energy resource.

## 6. Application to the Pentland Firth

### 6.1. Model Setup

The Pentland Firth model has a longitudinal resolution of 500m and a variable latitudinal resolution, approximately equal to 500m. The model domain extends from 1.3°W to 4°W and from 58.3°N to 60.3°N (Figure 8). Bathymetry for the Pentland Firth was provided by the *General*

284 *Bathymetric Chart of the Oceans* (GEBCO) 30 arc second data set. The  
 285 vertical resolution was defined by 10 sigma layers, providing a resolution of  
 286 approximately 3m in the Inner Sound. The model was nested inside a  
 287 North West European Shelf model which had a resolution of approximately  
 288 3km, with one-way  $M_2$  and  $S_2$  tidal elevation and tidal current forcing at  
 289 the boundaries. The validation of the outer model (full results not  
 290 presented here) for the semi-diurnal  $M_2$  and  $S_2$  tidal constituents were 17  
 291 cm and 5 cm for amplitude and  $2^\circ$  and  $6^\circ$  for phase when compared with 12  
 292 *in-situ* tide gauges. After the initial run without tidal energy extraction  
 293 (the control), the model was re-run with 2-D and 3-D tidal energy  
 294 extraction. A 300MW tidal array was implemented within the area of the  
 295 Inner Sound leased by the Crown Estate (Crown Estate, 2010).

#### 296 6.1.1. Model Validation

297 The  $M_2$  and  $S_2$  constituents separated using the harmonic analysis software  
 298 T\_TIDE (Pawlowicz et al., 2002), were compared with 9 tide gauges located  
 299 around the Orkney domain and the results given in Table 3. Additionally,  
 300 the depth averaged velocities at three ADCP locations (see Figure 8 a) were  
 301 validated following the principal components analysis method prescribed by  
 302 Boon (2004), (see Figure 9).

303 The RMSE for  $M_2$  and  $S_2$  amplitudes were 7 cm and 3 cm and for phase  
 304 were  $13^\circ$  and  $12^\circ$  with Scatter Index values of less than 10% for  $S_2$   
 305 amplitude and phase and  $\sim 6\%$  and  $\sim 12\%$  for  $M_2$  amplitude and phase  
 306 respectively.

307 The modelled depth averaged current amplitudes and phases were validated  
 308 using current and direction measurements from three 30 day ADCP

309 deployments. The devices were deployed within the centre channel of the  
 310 Pentland Firth by Guardline Surveys on behalf of the Navigation and  
 311 Safety branch of the Maritime and Coastguard Agency. Each mooring is  
 312 separated by  $\sim 8$ km. As would be expected, the modelled results show  
 313 much less variability than the observational data. Overall, it is promising to  
 314 observe that both magnitude and direction are reasonably represented by  
 315 the model. The RMSE of the tidal current speed amplitudes and phase for  
 316 the  $M_2$  and  $S_2$  constituents were 21 cm/s, 4 cm/s and  $5^\circ, 13^\circ$  respectively.

## 317 *6.2. Results for the baseline case*

318 The model was initially applied to a case with no tidal energy extraction,  
 319 hereafter referred to as the control scenario, in order to understand the  
 320 residual circulation and theoretical available kinetic energy before tidal  
 321 energy extraction. The mid-depth 3-D velocities from the regional ocean  
 322 model were integrated between depths of 10m and 20m (the diameter of the  
 323 turbines) to establish the control scenario flow dynamics. The mapped  
 324 hub-height integrated velocity field (m/s) shows the streaming of the tide  
 325 through the Pentland Firth between the islands of Stroma and Swona at  
 326 different stages of the tide (referenced to Wick), vectors indicate the flow  
 327 direction (Figure 10). On the spring flood tide this tidal jet is separated by  
 328 the Pentland Skerries, behind which an obvious eddy can be identified. The  
 329 tidal jet of Pentland Skerries doesn't propagate as far on the neap flood  
 330 tide and the reduced currents in the main channel lead to more resource  
 331 entering the sub-channels between Stroma and Swona where there is a  
 332 slight increase of current magnitude. During the ebb phase, the direction of  
 333 the tidal jet is reversed and fast currents are found at the tip of South

334 Ronaldsay and Dunnet Head. Figure 8 a, shows the locations of the leased  
 335 Pentland Firth tidal energy development sites: Brims (A), Brough Ness  
 336 (B), Ness of Duncansby (C) and Inner Sound (D). In this study, the tidal  
 337 arrays are located within the Inner Sound of Stroma, shown by the red  
 338 polygon in Figure 11. The Inner Sound of Stroma benefits from the  
 339 increased tidal streaming as a result of channel constraints and  
 340 subsequently is the most energetic of all the leased tidal stream sites. The  
 341 residual currents for depth-averaged tidal velocities over a spring-neap cycle  
 342 display a number of prominent eddies (Figure 11). The most noteworthy  
 343 eddies are located in the lee of the Pentland Skerries and the Isle of Stroma.

### 344 *6.3. Results for the energy extraction cases*

345 The results presented in this section are difference plots between the control  
 346 scenario and each individual extraction scenario and between the extraction  
 347 scenarios, i.e where the tidal energy extraction simulations are individually  
 348 extracted from the control simulation, and the 3-D simulation is subtracted  
 349 from the 2-D simulation. In the region of energy extraction, the magnitude  
 350 of velocity averaged over a spring-neap cycle was reduced by approximately  
 351 7cm/s for the 2-D extraction (Figure 12a) and 5cm/s for the 3-D extraction  
 352 case (Figure 12b). The change in velocity is greatest in close proximity to  
 353 the array, however, effects can be seen over the entirety of the model  
 354 domain as is consistent with other studies Neill et al. (2012). The flow in  
 355 the main channel of the Pentland Firth is increased by around 5cm/s, but  
 356 interestingly, the velocities at the other 3 tidal development zones is  
 357 reduced. On the whole, the impact on the velocities is greater using 2-D  
 358 extraction methods than when using the 3-D method (Figure 12c). The



variation in the mean surface, mid-depth and bottom currents is shown in Figure 13, where every 6th vector is plotted for clarity. In the mid-depths, current speed within the area of the array is 10cm/s slower for the 3-D case than for the 2-D case, and through the main channel is a 5cm/s increase in current speeds. In contrast, the surface layers of the water column see a  $> 10\text{cm/s}$  increase in current speeds within the area of the array. The bottom layer also sees a similar increase in current speed, although not over as large an area, concentrated around the tip of Mell's head. The bottom velocities are constrained by the bottom drag coefficient, hence a much smaller change in velocity is observed in this layer than in the surface layer. The vectors show differences between the methods in the current directions and eddy fields within the Inner Sound, for the surface and bottom layers of the water column. The percentage difference in bed shear stress between the methods is calculated and differences less than 10% are masked out (Figure 14). Positive values indicate regions where bed shear stresses are greater for the 3-D scenario. The resultant pattern is complex and highlights the non-linearities between the interaction of the hydrodynamics and the tidal array. Overall, the 3-D extraction scenario leads to higher bed shear stresses than the 2-D extraction scenario.

## 7. Discussion

A 3-D ROMS model has been used to compare tidal energy extraction modelling techniques and highlight the importance of using 3-D models for resource assessments. To simulate depth-averaged tidal energy extraction techniques within a 3-D ROMS model, a scaled thrust force is applied over

the entirety of the water column at a single location within an idealised channel. For 3-D tidal extraction, a method originally developed and validated by Roc et al. (2013) for ROMS is used. Here the turbine thrust force is applied over a vertical region of the water-column characterised by the diameter of the turbine, located at the mid-point of the water column at a single location within an idealised channel. The idealised channel experiment ensured that both techniques were comparable and led to the same reduction of velocity across the turbine area. After which both methods were applied to the leased Inner Sound development zone within a regional model of the Pentland Firth. The control Pentland Firth scenario was validated using ADCP and tide gauge measurements throughout the domain. The validation results show that the model errors for amplitude and phase are less than 10% of the tidal regime, and is thus considered suitable to compare tidal array modeling methods.

Our comparison of tidal energy extraction modeling techniques reveals that using a 2-D method to extract energy from the water column leads to a misrepresentation of the surface and bottom flow fields (Figure 3). The flow beneath the turbine is of particular importance as it is constrained between the turbine and seabed so could have quite considerable implications for sediment transport investigations (i.e. Fairley et al. (2015)). Little research has been published on wave-current interaction around tidal arrays however it is understood that incoming wave direction could have quite a significant impact on tidal resource so efforts made to implement 3-D tidal energy extraction would reduce uncertainty in these estimations (Hashemi et al., 2015; Lewis et al., 2014a).

408 The results from the idealised channel model suggest that depth-averaged  
 409 models can be misleading, when the depth averaged velocities are compared  
 410 for both methods, both methods appear to reduce the tidal flow by an  
 411 identical amount (Figure 2). However, upon comparing the 3-D profiles, the  
 412 velocity reduction in the location of the turbine is much greater, suggesting  
 413 an uncertainty in resource assessments between 20% and 25% (Table 2;  
 414 Figure 3). Traditional 2-D extraction methods where an increased frictional  
 415 force is applied at the sea-bed cause the near-bed velocity to reduce, this is  
 416 not the case with the actuator disc method where the velocities will  
 417 increase as they by-pass the region of extraction. Future generations of  
 418 tidal energy development are likely to look to deeper water environments  
 419 and 3-D modelling techniques will be vital for reducing the uncertainty in  
 420 resource assessments.

421 Located below the main residual circulation patterns (Figure 11) within the  
 422 channel are a number of sandbanks (Chatzirodou and Karunarathna, 2014).  
 423 Sandbanks are of significant importance to shallow water regions where  
 424 their presence enhances wave dissipation and refraction which in some cases  
 425 provides natural protection to the shoreline (Neill et al., 2012; Dyer and  
 426 Huntley, 1999; Lewis et al., 2014b). In some regions they are of significant  
 427 economical importance and these quiescent regions can provide important  
 428 feeding grounds for fish and have high ecological significance for benthic  
 429 communities (Chatzirodou and Karunarathna, 2014). Understanding how  
 430 these regions might change as a result of tidal stream energy extraction is  
 431 subsequently of high importance and will be the emphasis of future work.  
 432 Although the Pentland Firth is a channel and thus might be expected to

433 have rectilinear currents, some misalignment and flow asymmetry can be  
 434 observed, as hypothesised by Lewis et al. (2015) (Figure 10). Interestingly,  
 435 for both extraction scenarios, there is asymmetry in the flow behavior  
 436 either side of the Inner Sound. We see a decrease in flow propagating out of  
 437 the Inner Sound into the North Sea, however, a clear increase in flow can be  
 438 seen either side of the array particularly where it becomes constrained  
 439 between the array and the coastline (Figure 12). Extraction of energy in  
 440 regions of tidal asymmetry has been shown to have a greater impact on  
 441 sediment transport than areas where flood and ebb tides are symmetrical  
 442 (Neill et al., 2009). Extracting energy from the Inner Sound affects the  
 443 current magnitude at the other three sites within the Pentland Firth - a  
 444 more detailed study into the changes to hydrodynamics at these sites will  
 445 be required to fully characterise the effect on the resource. 3-D energy  
 446 extraction methods will help improve the quantification of the impact of  
 447 tidal energy extraction on sea-bed processes (Figure 3; Bahaj et al. (2007)).  
 448 A number of studies have established that small tidal stream developments  
 449 are likely to have a minimal effect on sediment dynamics (Robins et al.,  
 450 2014; Fairley et al., 2015). The 3-D extraction case had a greater impact on  
 451 the velocities within the vicinity of the array, however the 2-D method  
 452 appears to remove more kinetic energy from the domain (Figure 12).  
 453 Studies seeking optimal turbine array design tend to settle upon a tidal  
 454 fence design (i.e Adcock et al. (2013)), the increased levels of extraction  
 455 and impacts on flow from these arrays will have a greater impact on the  
 456 flow dynamics than those presented here. Nevertheless, from Figure 13, if  
 457 we consider the velocities within the bottom most depth layer, the 3-D

method has the fastest near-bed velocities during the flood tide by a margin exceeding 10cm/s. Bed shear stresses are related to velocity squared and thus justifies the importance of defining the turbines as a mid-depth force-term (Soulsby, 1997).

This research provides a comparison of the methods used to model tidal energy extraction in regional models, nevertheless further research would be required to quantify the error between resource assessment models. Further questions remain as to whether device resolving methods are appropriate within regional models, this would involve improvements to model efficiency and resolution to take into account turbine array design and turbine induced turbulence. There is a clear knowledge gap with regards to feedbacks between tidal stream devices and regional hydrodynamics, since little observational data is available for the validation of device resolving models. Additionally, there are many ways in which modelling the resource could be improved, taking into account the interaction of waves with the tidal stream resource and array development, and the consequences of tidal energy developments upon neighboring tidal energy development sites. These additions would come at a high computational cost but one which is within the realm of current high performance computing technology.

## 8. Conclusions

Although observational measurements are key for model validation and for characterising the resource, they are costly and unable to account for spatial variations. Hence, numerical modelling tools are essential within the tidal energy industry for resource and environmental impact assessments.

482 We find a 3-D modeling approach is necessary to resolve vertical flow  
 483 bypass around the turbine and are therefore key to reducing bias in  
 484 resource and environmental impact assessments. Using the 3-D method,  
 485 velocities across the extraction region are between 20% and 25% less than  
 486 they are for the 2-D method. This research showed that as water depth  
 487 increased the discrepancy in velocity at the disk between the two methods  
 488 also increased, suggesting that there are greater uncertainties associated  
 489 with resource assessments with 2-D models in deeper water. Additionally it  
 490 was found that velocities between the turbine and the sea bed for the 3-D  
 491 method exceed those in the same region for the 2-D method by more than  
 492 10%, suggesting that depth-averaged models assessing the impacts on  
 493 sediment pathways could be greatly under-estimating the levels of sediment  
 494 transport. Moreover, the vertical structure of the flow is essential to resolve  
 495 to reduce uncertainties within power calculations, particularly where water  
 496 depths exceed 30m. Therefore, depth-averaged models - which are  
 497 computationally more efficient - are useful tools for a first order of  
 498 approximation of resource but for accurate assessments of resource  
 499 interaction with tidal devices 3-D models are required. The use of 3-D  
 500 models will further reduce the uncertainty in physical environmental impact  
 501 assessments which would aid the development of the tidal stream industry.

## 502 9. Acknowledgements

503 Alice Goward Brown wishes to acknowledge Fujitsu and HPC Wales for  
 504 their role in funding and providing computational support throughout this  
 505 PhD research. Simon Neill and Matt Lewis would like to acknowledge the

support of the Welsh Government NRN-LCEE scheme through the  
QUOTIENT project.

## References

- G. D. Egbert, R. D. Ray, Estimates of M2 tidal energy dissipation from TOPEX/Poseidon altimeter data, *Journal of Geophysical Research: Oceans* 106 (C10) (2001) 22475–22502.
- B. K. Arbic, C. Garrett, A coupled oscillator model of shelf and ocean tides, *Continental Shelf Research* 30 (6) (2010) 564574.
- S. Hartwell-Naguib, R. Benwell, M. O'Brien, J. Bird, F. Grahah, J. Wright J.Oand Evans, N. Davies, The Future of Marine Renewables in the UK - Energy and Climate Change .
- S. P. Neill, A. Vögler, A. J. Goward-Brown, S. Baston, M. J. Lewis, P. A. Gillibrand, S. Waldman, D. K. Woolf, The wave and tidal resource of Scotland, *Renewable Energy* .
- R. O. Murray, A. Gallego, A modelling study of the tidal stream resource of the Pentland Firth, Scotland, *Renewable Energy* 102 (2017) 326–340.
- S. J. Couch, I. Bryden, Tidal current energy extraction: hydrodynamic resource characteristics, *Proceedings of the Institution of Mechanical Engineers, Part M: Journal of Engineering for the Maritime Environment* 220 (4) (2006) 185194.

- 526 I. Bryden, G. T. Melville, Choosing and evaluating sites for tidal current  
527 development, Proceedings of the Institution of Mechanical Engineers,  
528 Part A: Journal of Power and Energy 218 (8) (2004) 567577.
- 529 B. Polagye, J. Epler, J. Thomson, Limits to the predictability of tidal  
530 current energy, in: OCEANS 2010, IEEE, 1–9, 2010.
- 531 D. Prandle, The vertical structure of tidal currents and other oscillatory  
532 flows, Continental Shelf Research 1 (2) (1982) 191–207.
- 533 L. Blunden, A. Bahaj, Tidal energy resource assessment for tidal stream  
534 generators, Proceedings of the Institution of Mechanical Engineers, Part  
535 A: Journal of Power and Energy 221 (2) (2007) 137–146.
- 536 T. A. Adcock, S. Draper, T. Nishino, Tidal power generation—A review of  
537 hydrodynamic modelling, Proceedings of the Institution of Mechanical  
538 Engineers, Part A: Journal of Power and Energy (2015)  
539 0957650915570349.
- 540 P. E. Robins, S. P. Neill, M. J. Lewis, Impact of tidal-stream arrays in  
541 relation to the natural variability of sedimentary processes, Renewable  
542 Energy 72 (2014) 311–321.
- 543 S. Draper, G. Houlsby, M. Oldfield, A. Borthwick, Modelling tidal energy  
544 extraction in a depth-averaged coastal domain, IET renewable power  
545 generation 4 (6) (2010) 545554.
- 546 R. Ahmadian, R. Falconer, B. Bockelmann-Evans, Far-field modelling of  
547 the hydro-environmental impact of tidal stream turbines, Renewable  
548 Energy 38 (1) (2012) 107116.



- 549 S. D. G. H. M. Oldfield, A. Borthwick, Modelling tidal energy extraction in  
550 a depth-averaged coastal domain .
- 551 M. Lewis, S. Neill, P. Robins, M. Hashemi, Resource assessment for future  
552 generations of tidal-stream energy arrays, *Energy* 83 (2015) 403–415.
- 553 S. P. Neill, M. R. Hashemi, M. J. Lewis, The role of tidal asymmetry in  
554 characterizing the tidal energy resource of Orkney, *Renewable Energy* 68  
555 (2014) 337350.
- 556 S. P. Neill, J. R. Jordan, S. J. Couch, Impact of tidal energy converter  
557 (TEC) arrays on the dynamics of headland sand banks, *Renewable*  
558 *Energy* 37 (1) (2012) 387397.
- 559 I. G. Bryden, S. J. Couch, A. Owen, G. Melville, Tidal current resource  
560 assessment, *Proceedings of the Institution of Mechanical Engineers, Part*  
561 *A: Journal of Power and Energy* 221 (2) (2007) 125–135, ISSN 0957-6509,  
562 2041-2967.
- 563 Z. Yang, T. Wang, A. E. Copping, Modeling tidal stream energy extraction  
564 and its effects on transport processes in a tidal channel and bay system  
565 using a three-dimensional coastal ocean model, *Renewable Energy* 50  
566 (2013) 605613.
- 567 M. Harrison, W. Batten, L. Myers, A. Bahaj, Comparison between CFD  
568 simulations and experiments for predicting the far wake of horizontal axis  
569 tidal turbines, *Renewable Power Generation, IET* 4 (6) (2010) 613627.
- 570 M. A. Shields, D. K. Woolf, E. P. Grist, S. A. Kerr, A. C. Jackson, R. E.  
571 Harris, M. C. Bell, R. Beharie, A. Want, E. Osalusi, Marine renewable

- energy: The ecological implications of altering the hydrodynamics of the  
marine environment, *Ocean & Coastal Management* 54 (1) (2011) 29.
- G. Shapiro, Effect of tidal stream power generation on the region-wide  
circulation in a shallow sea, *Ocean Science* 7 (2011) 165174.
- A. S. Bahaj, L. E. Myers, M. D. Thomson, N. Jorge, Characterising the  
wake of horizontal axis marine current turbines, *Proc. 7th EWTEC*.
- L. Myers, A. Bahaj, Simulated electrical power potential harnessed by  
marine current turbine arrays in the Alderney Race, *Renewable Energy*  
30 (11) (2005) 17131731.
- T. Roc, D. C. Conley, D. Greaves, Methodology for tidal turbine  
representation in ocean circulation model, *Renewable Energy* 51 (2013)  
448–464, ISSN 09601481.
- C. Vogel, R. Willden, G. Houlsby, A correction for depth-averaged  
simulations of tidal turbine arrays, in: *Proceedings of the 10th European  
Wave and Tidal Energy Conference (EWTEC)*, Aalborg, Denmark,  
vol. 25, 2013.
- K. Thyng, J. Riley, Idealized headland simulation for tidal hydrokinetic  
turbine siting metrics, in: *OCEANS 2010, IEEE*, 16, 2010.
- P. E. Robins, S. P. Neill, M. J. Lewis, S. L. Ward, Characterising the  
spatial and temporal variability of the tidal-stream energy resource over  
the northwest European shelf seas, *Applied Energy* 147 (2015) 510–522.

- 593 A. F. Shchepetkin, J. C. McWilliams, The regional oceanic modeling system  
594 (ROMS): a split-explicit, free-surface, topography-following-coordinate  
595 oceanic model, *Ocean Modelling* 9 (4) (2005) 347–404.
- 596 J. C. Ohlmann, S. Mitarai, Lagrangian assessment of simulated surface  
597 current dispersion in the coastal ocean, *Geophysical Research Letters*  
598 37 (17).
- 599 J. Warner, B. Armstrong, R. He, J. Zambon, Development of a Coupled  
600 OceanAtmosphereWaveSediment Transport (COAWST) Modeling  
601 System, *Ocean modelling* 35 (3) (2010) 230244.
- 602 M. Sánchez, R. Carballo, V. Ramos, G. Iglesias, Tidal stream energy  
603 impact on the transient and residual flow in an estuary: A 3D analysis,  
604 *Applied Energy* 116 (2014) 167177.
- 605 M. E. Harrison, W. M. J. Batten, L. E. Myers, A. S. Bahaj, A Comparison  
606 between CFD simulation and experiments for predicting the far wake of  
607 horizontal axis tidal turbines, 8th European Wave and Tidal Energy  
608 Conf, Uppsala, Sweden .
- 609 S. Baston, R. E. Harris, D. K. Woolf, R. A. Hiley, J. C. Side, Sensitivity  
610 Analysis of the Turbulence Closure Models in the Assessment of Tidal  
611 Energy Resource in Orkney, in: 10th European Wave and Tidal Energy  
612 conference, Aalborg, Denmark, 2013.
- 613 J. Whelan, J. Graham, J. Peiro, A free-surface and blockage correction for  
614 tidal turbines, *Journal of Fluid Mechanics* 624 (2009) 281–291.

- 615 M. C. Easton, D. K. Woolf, P. A. Bowyer, The dynamics of an energetic  
616 tidal channel, the Pentland Firth, Scotland, Continental Shelf Research .  
617 Crown Estate, Leasing round and projects, URL  
618 <http://www.thecrownestate.co.uk>, 2010.
- 619 MeyGen, UK leads marine energy revolution as worlds largest tidal stream  
620 project agrees investment to begin construction in Scotland, URL  
621 <http://www.meygen.com/the-project/meygen-news/>, 2010.
- 622 The Carbon Trust, Tech. Rep., 2011.
- 623 R. Pawlowicz, B. Beardsley, S. Lentz, Classical tidal harmonic analysis  
624 including error estimates in MATLAB using T-TIDE, Computers &  
625 Geosciences 28 (8) (2002) 929–937.
- 626 J. D. Boon, Secrets of the Tide: Tide and Tidal Current Analysis and  
627 Applications, Storm Surges and Sea Level Rise, Chichester (UK):  
628 Horwood Publishing, 2004.
- 629 I. Fairley, I. Masters, H. Karunaratna, The cumulative impact of tidal  
630 stream turbine arrays on sediment transport in the Pentland Firth,  
631 Renewable Energy 80 (2015) 755–769.
- 632 M. R. Hashemi, S. P. Neill, P. E. Robins, A. G. Davies, M. J. Lewis, Effect  
633 of waves on the tidal energy resource at a planned tidal stream array,  
634 Renewable Energy 75 (2015) 626–639.
- 635 M. Lewis, S. Neill, M. Hashemi, M. Reza, Realistic wave conditions and

- 636 their influence on quantifying the tidal stream energy resource, *Applied*  
637 *Energy* 136 (2014a) 495–508.
- 638 A. Chatzirodou, H. Karunaratna, Impacts of tidal energy extraction on  
639 sea bed morphology, *Coastal Engineering Proceedings* 1 (34) (2014) 33.
- 640 K. R. Dyer, D. A. Huntley, The origin, classification and modelling of sand  
641 banks and ridges, *Continental Shelf Research* 19 (10) (1999) 12851330.
- 642 M. Lewis, S. Neill, A. Elliott, Interannual variability of two offshore sand  
643 banks in a region of extreme tidal range, *Journal of Coastal Research*  
644 31 (2) (2014b) 265–275.
- 645 S. Neill, E. Litt, S. Couch, A. Davies, The impact of tidal stream turbines  
646 on large-scale sediment dynamics, *Renewable Energy* 34 (12) (2009)  
647 28032812.
- 648 T. A. Adcock, S. Draper, G. T. Houlsby, A. G. Borthwick, S. Serhadlolu,  
649 The available power from tidal stream turbines in the Pentland Firth,  
650 *Proceedings of the Royal Society A: Mathematical, Physical and*  
651 *Engineering Science* 469 (2157).
- 652 R. Soulsby, *Dynamics of marine sands: a manual for practical applications*,  
653 Thomas Telford, 1997.

654 **Tables**

655 **Figures**

Table 1: Comparison between mid-depth velocity ( $U$ ) and depth averaged velocity ( $\bar{U}$ ) for both 2-D and 3-D extraction scenarios.

	3-D Method		2-D Method	
	U-velocity	$\bar{U}$ velocity	U-velocity	$\bar{U}$ velocity
$T_D$ (m)	10	10	30	30
$U_{IN}$ (m/s)	2.04	2.00	2.04	2.00
$U_{OUT}$ (m/s)	2.02	1.99	2.03	1.99
$U_D$ (m/s)	1.55	1.81	1.80	1.81

Table 2: Velocity and power difference between the two methods with increasing channel depth.

Channel depth (m)	Free stream velocity (m/s)	Velocity at turbine (m/s)		Velocity difference (m/s)	Maximum Power density difference (kW/m <sup>2</sup> )
		2D	3D		
30	2	1.86	1.46	0.4	1.7
60	2	1.87	1.44	0.43	2.2
90	2	1.88	1.4	0.48	2.6

Table 3: Observed and modelled amplitudes ( $H$ , in meters) and phases ( $g$ , in degrees) of the  $M_2$  and  $S_2$  tidal constituents for the 9 tide gauges represented by red crosses in Figure 8. The principle tide gauge is identified in bold font.

Station	Observed				Modelled			
	<b>M2</b>		<b>S2</b>		<b>M2</b>		<b>S2</b>	
	H (m)	$g(^{\circ})$	H (m)	$g(^{\circ})$	H (m)	$g(^{\circ})$	H (m)	$g(^{\circ})$
<b>Wick</b>	<b>1.02</b>	<b>322</b>	<b>0.35</b>	<b>0</b>	<b>1.02</b>	<b>312.31</b>	<b>0.37</b>	<b>353.51</b>
Burwick	0.88	287	0.35	322	0.81	289.39	0.30	326.77
Gills Bay	1.12	268	0.41	300	1.09	263.14	0.41	297.77
Scrabster	1.35	247	0.51	280	1.26	241.25	0.49	276.01
Kirkwall	0.84	301	0.29	339	0.91	278.26	0.34	315.64
Loth	0.74	300	0.26	336	0.85	279.67	0.32	316.96
Kettletoft Pier	0.92	312	0.33	347	0.85	301.24	0.32	339.69
Tingwall	0.86	276	0.31	310	0.90	271.16	0.33	308.22
Stromness	0.89	270	0.35	303	0.87	252.43	0.34	288.56
	<b>RMSE</b>				<b>0.07</b>	<b>13.06</b>	<b>0.03</b>	<b>11.83</b>
	<b>SI(%)</b>				<b>6.39</b>	<b>12.13</b>	<b>9.11</b>	<b>8.24</b>

Figure 1: Illustrated comparison of the consequent vertical tidal current profiles if 2-D (solid line) or 3-D (dashed line) turbine modelling methods are used in 3-D ocean models.

Figure 2: Comparison of horizontal velocity along the channel domain for both 2-D and 3-D scenarios.

Figure 3: Vertical flow bypass around the 3-D turbine (a) and through the 2-D turbine (b).  $X$  is scaled by the turbine diameter ( $X/T_D$ ).

Figure 4: Power density for (a) the 3-D method, (b) the 2-D method and (c) the power difference between the two methods in a channel of 30m.

Figure 5: Power density for (a) the 3-D method, (b) the 2-D method and (c) the power difference between the two methods in a channel of 60m.

Figure 6: Power density for (a) the 3-D method, (b) the 2-D method and (c) the power difference between the two methods in a channel of 90m.

Figure 7: Orkney model domain. Cotidal lines link locations of equal tidal phase ( $^{\circ}$ ) for  $M_2$  (a) and  $S_2$  (b) tidal elevation. The tidal amplitude is indicated by the colour scale (m).

Figure 8: (a) Orkney model domain showing ADCP locations (green triangles), tide gauge locations (red crosses). Inset is the Pentland Firth with polygons displaying the regions allocated by the crown estate for tidal energy development. Bathymetry contours show spatial distribution of water depth over the model grid. (b) Comparison of modelled (x) and observed (y)  $M_2$  and  $S_2$  amplitudes and phases for velocity (green triangles) and elevation (red crosses).



Figure 9: Tidal ellipses for the modelled (a,b and c) and observed (d, e and f) tidal currents at each ADCP location.

Figure 10: Tidal streaming within the Pentland Firth when it is peak spring flood and ebb tides (red diamonds) and neap flood and ebb tides (black cross) at Wick. Colours show velocity magnitude at the mid-depth, and vectors show current direction.

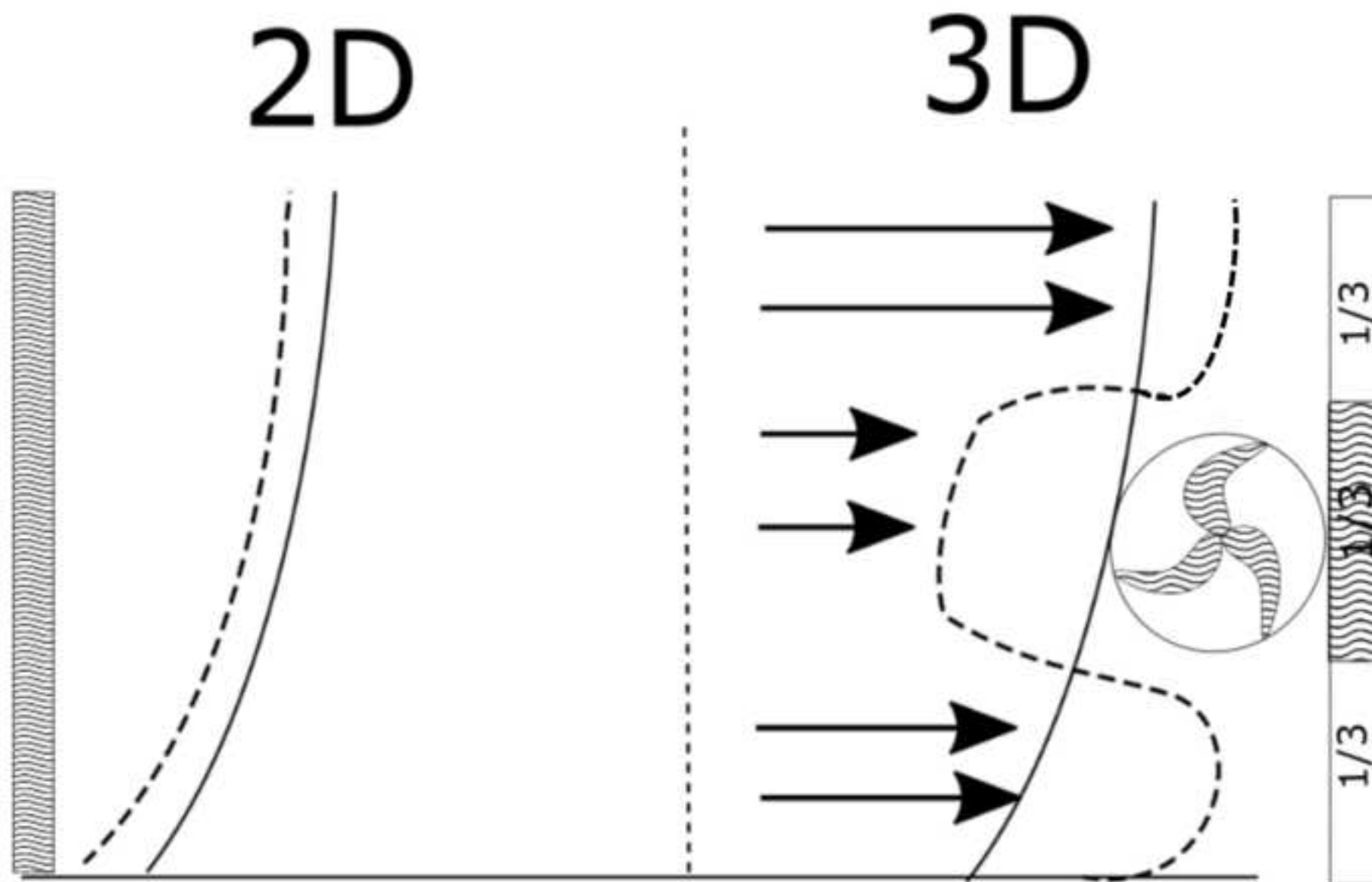
Figure 11: Modelled residual tidal currents in the Pentland Firth for the control scenario. The red polygon indicates the location of the Inner Sound tidal array and the contours represent the water depth (m).

Figure 12: Change in magnitude of velocity (cm/s), due to energy extraction over a spring-neap cycle between (a) the control and 2-D extraction scenario, (b) the control and 3-D extraction scenario and (c) 2-D and 3-D extraction scenarios. Black polygon shows the location of the turbine array for each case.

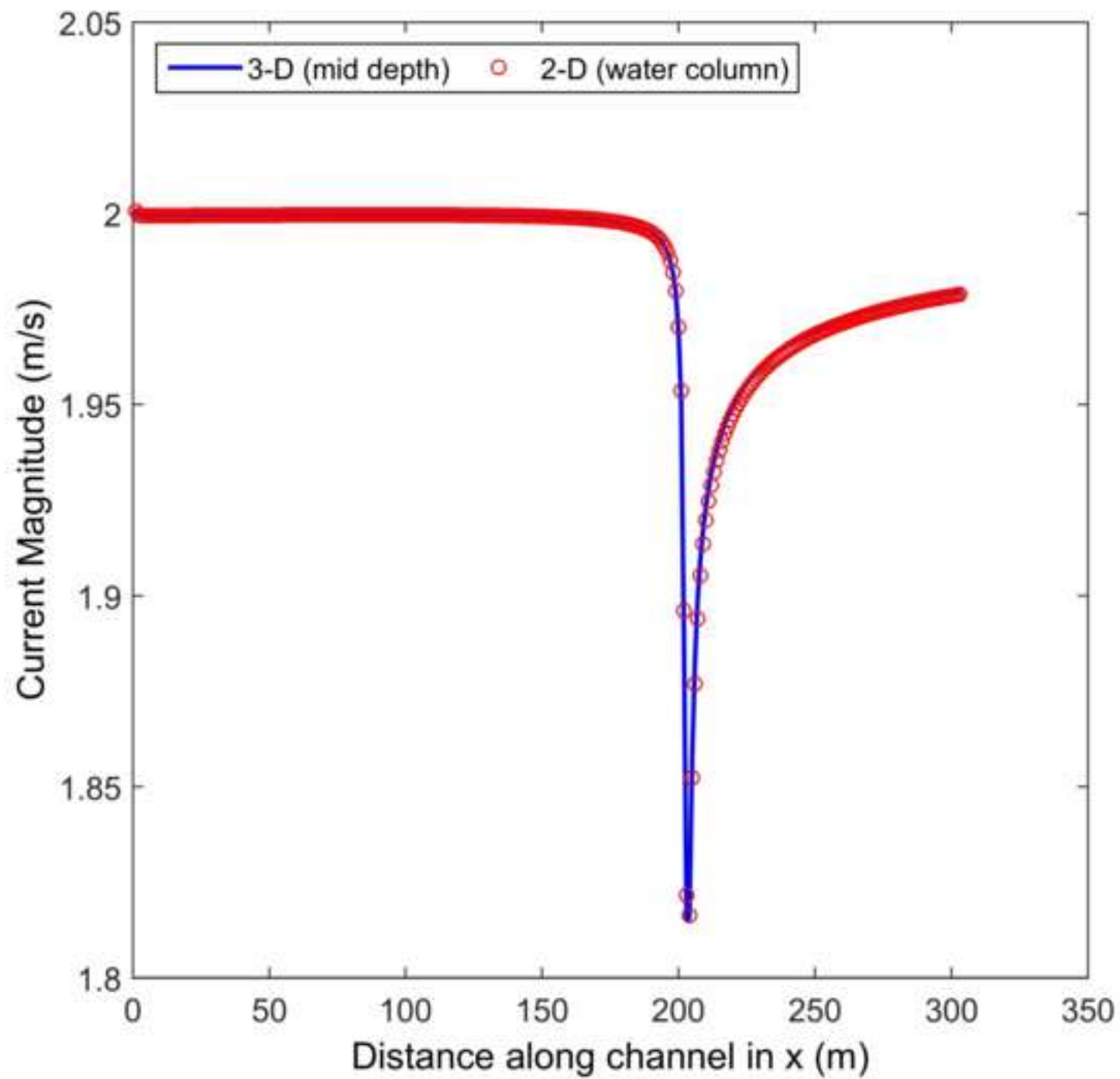
Figure 13: Comparison of mean surface, mid-depth and bottom currents for 2-D and 3-D extraction simulations.

Figure 14: Percentage change in magnitude of bed shear stress between 3-D and 2-D extraction scenarios over a spring-neap cycle. Black polygon shows the location of the turbine array.

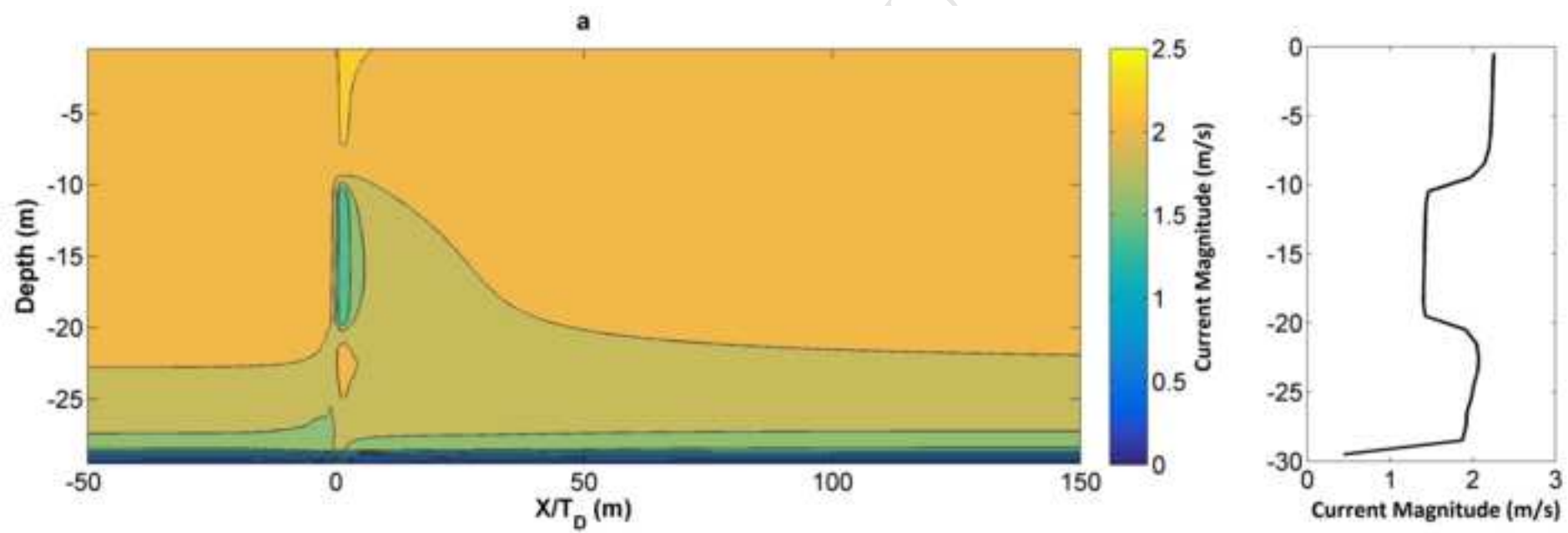
Figure



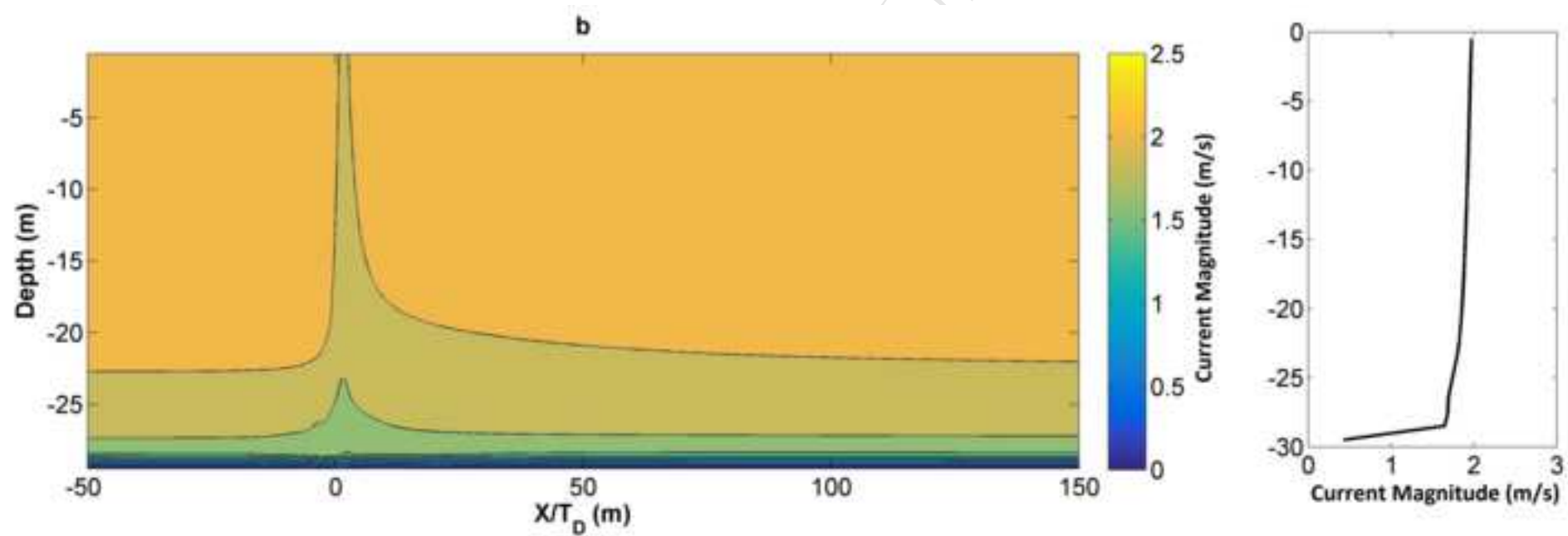
Figure



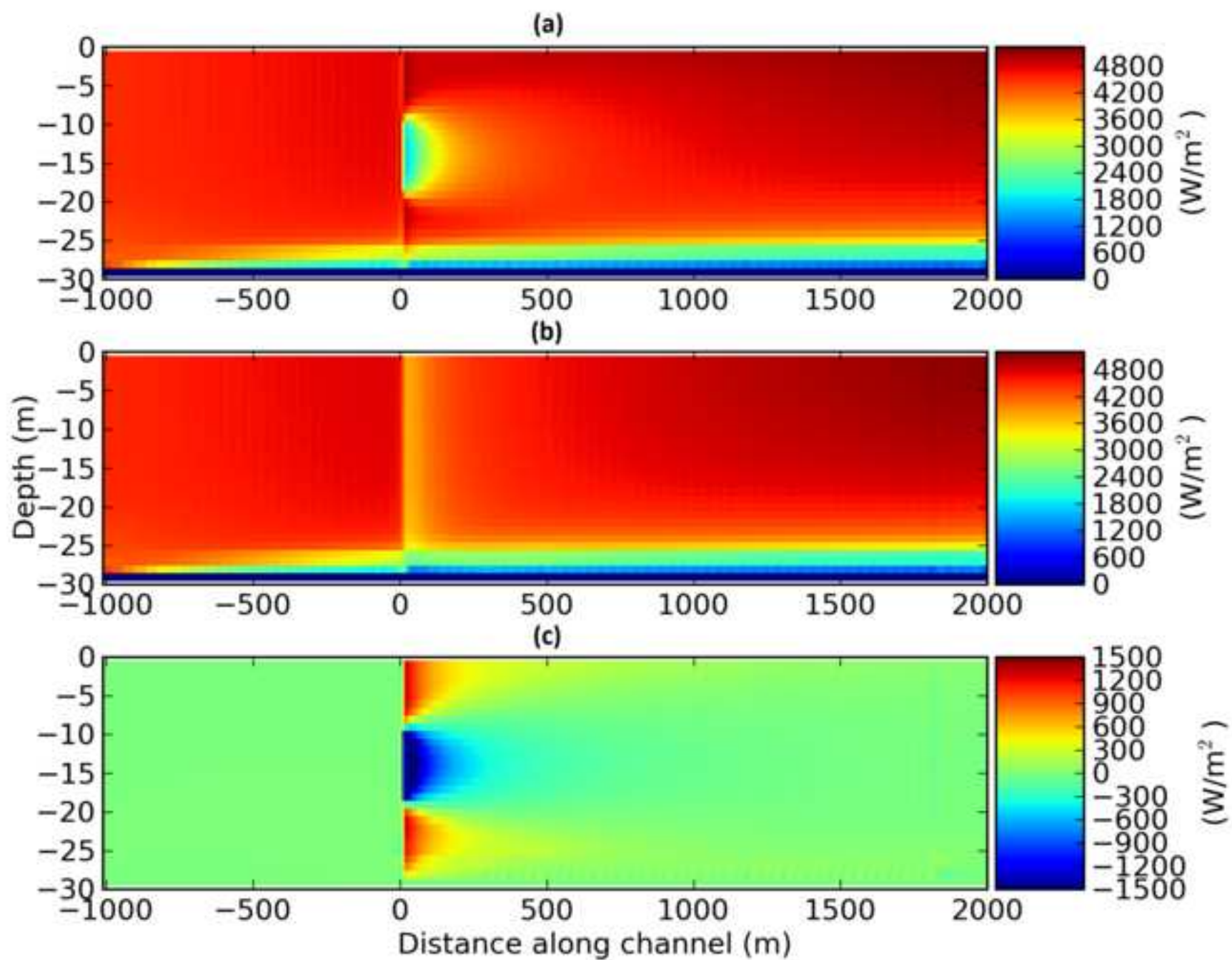
Figure



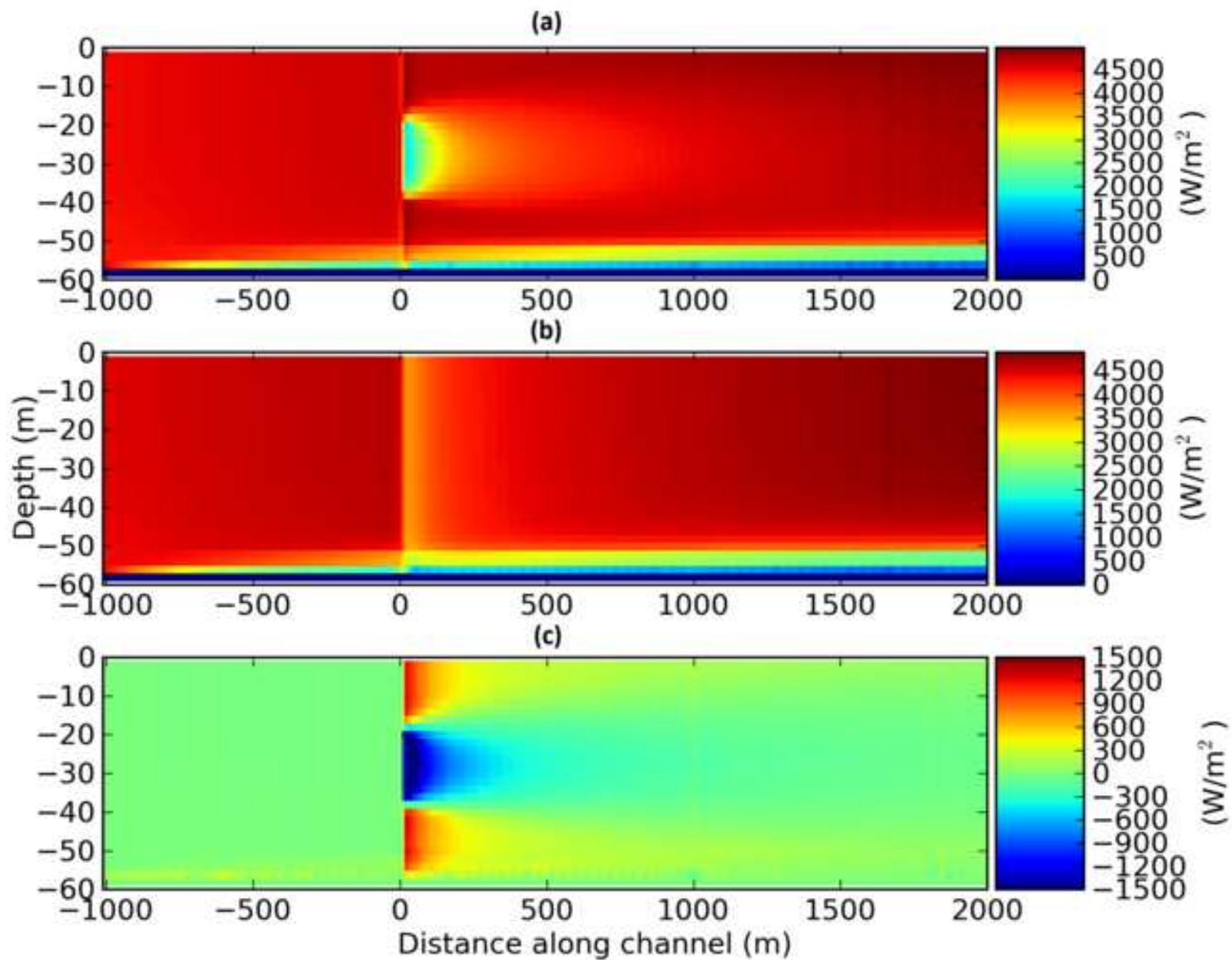
Figure



Figure

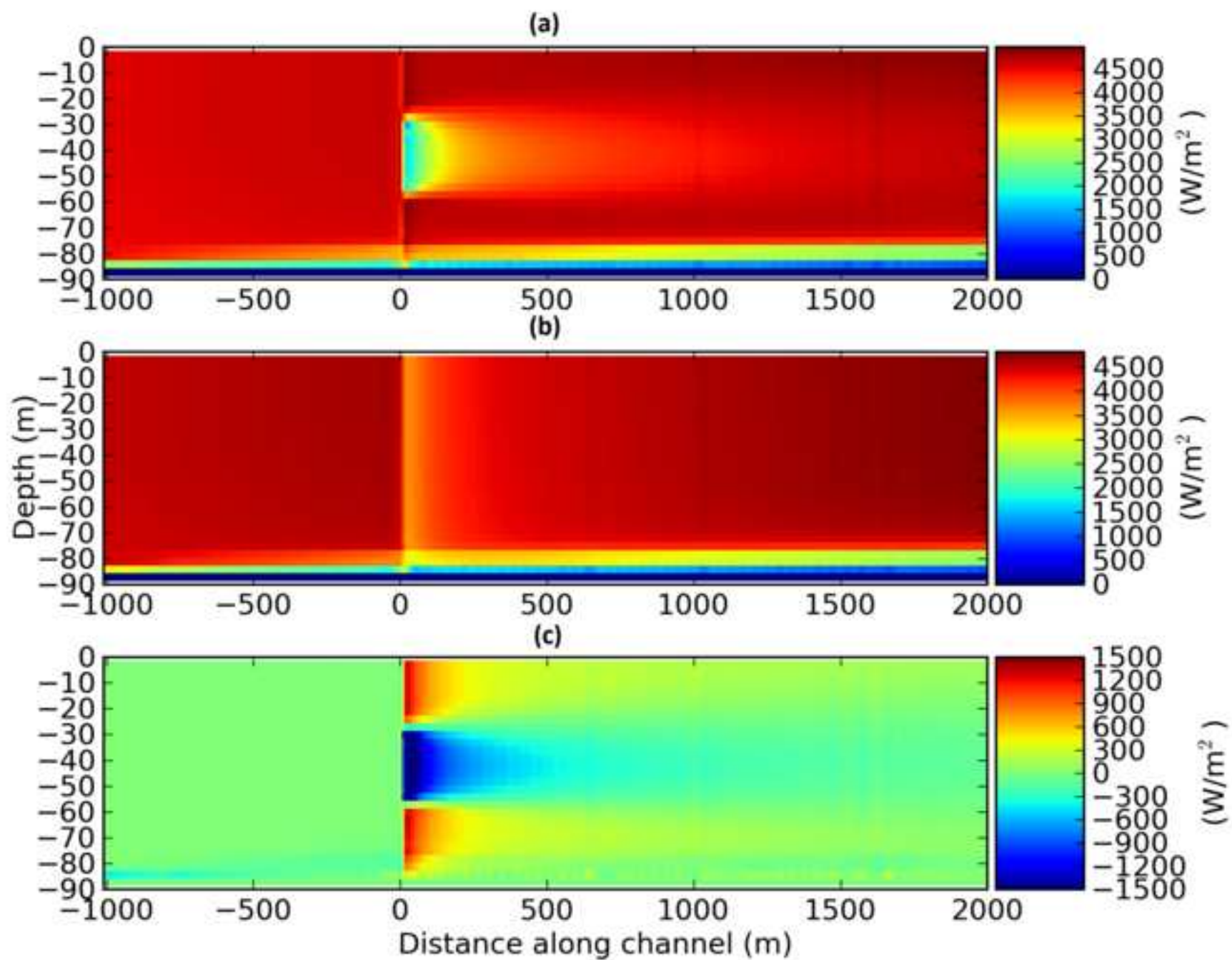


Figure



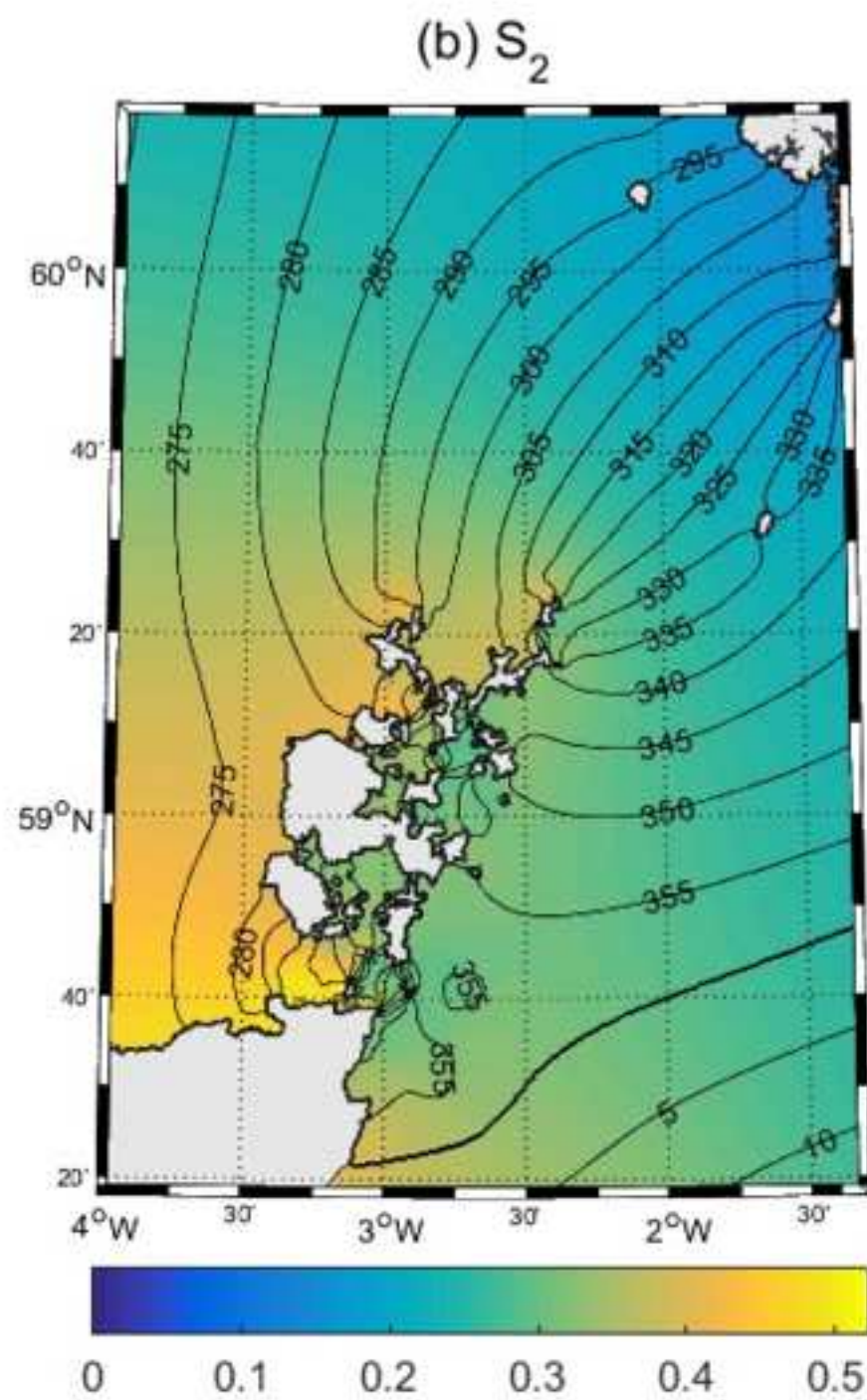
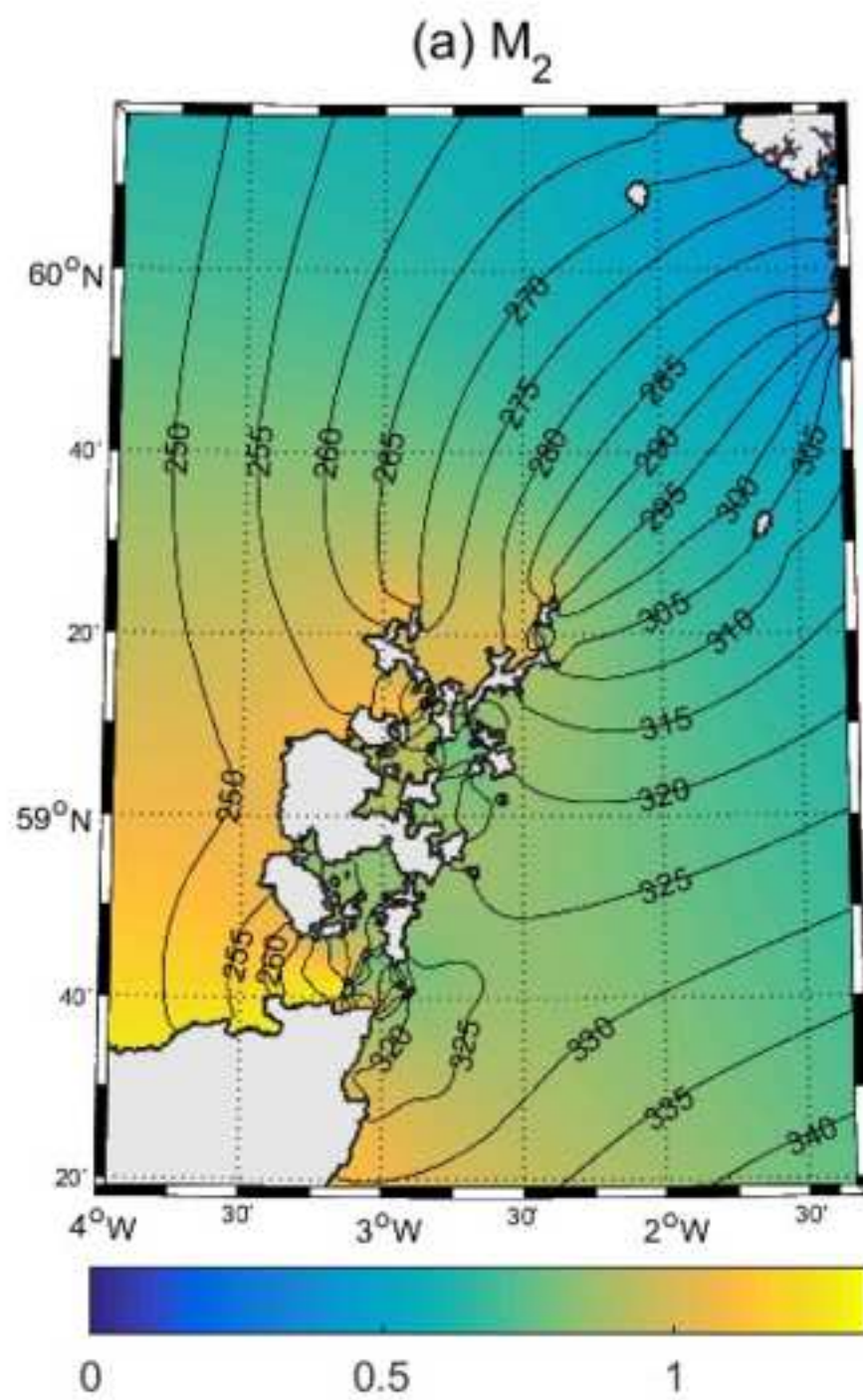


Figure

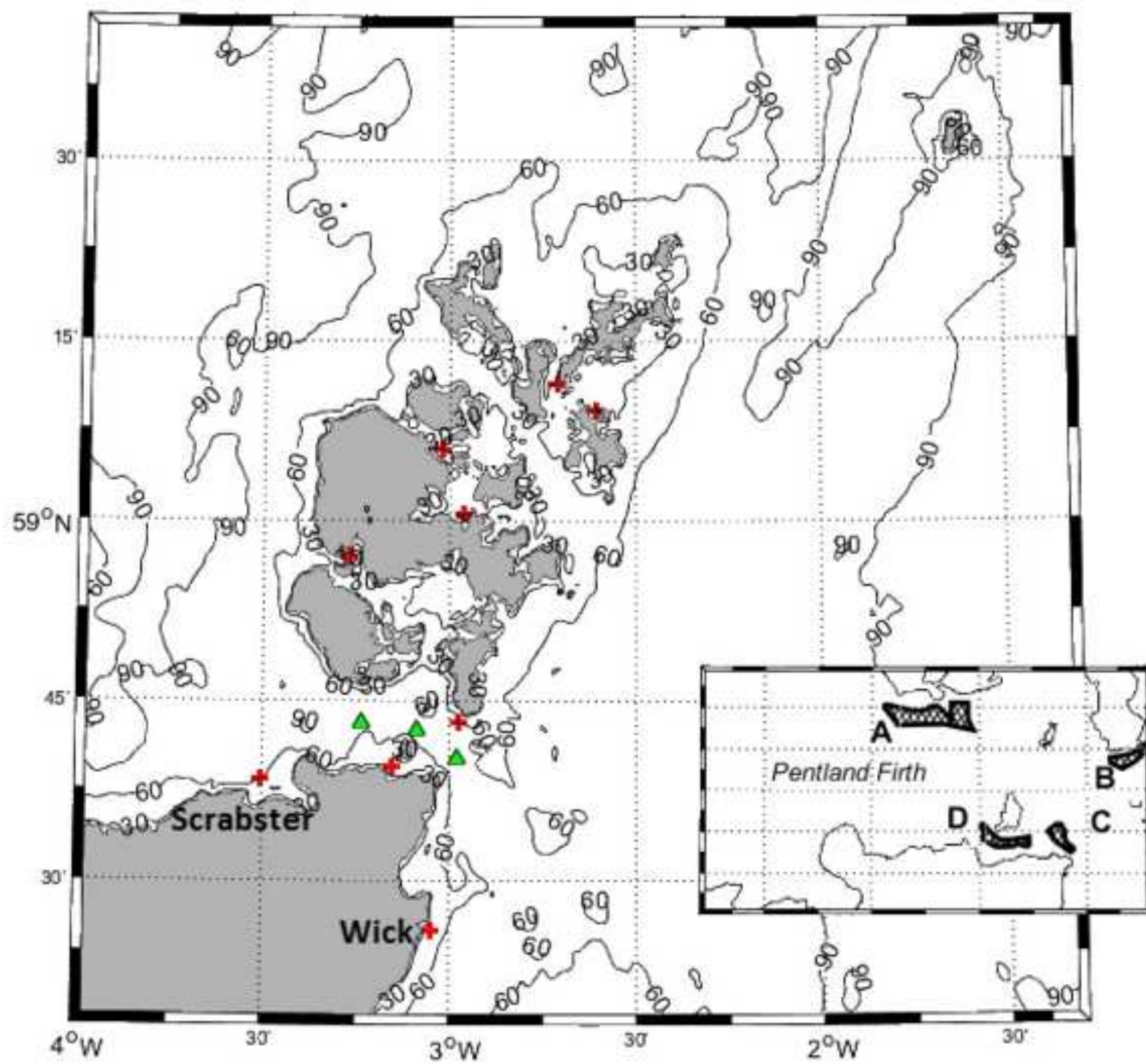


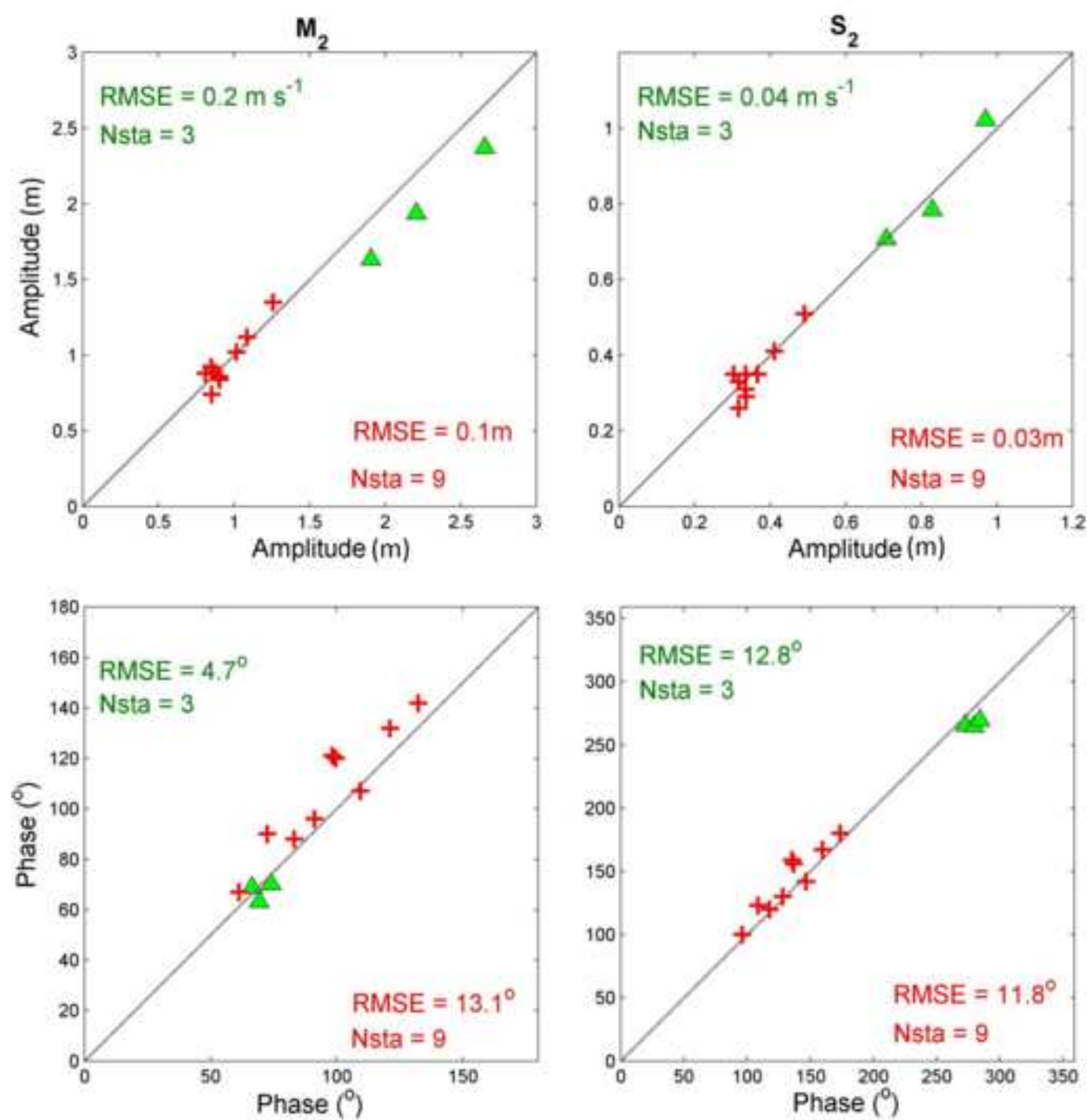


Figure



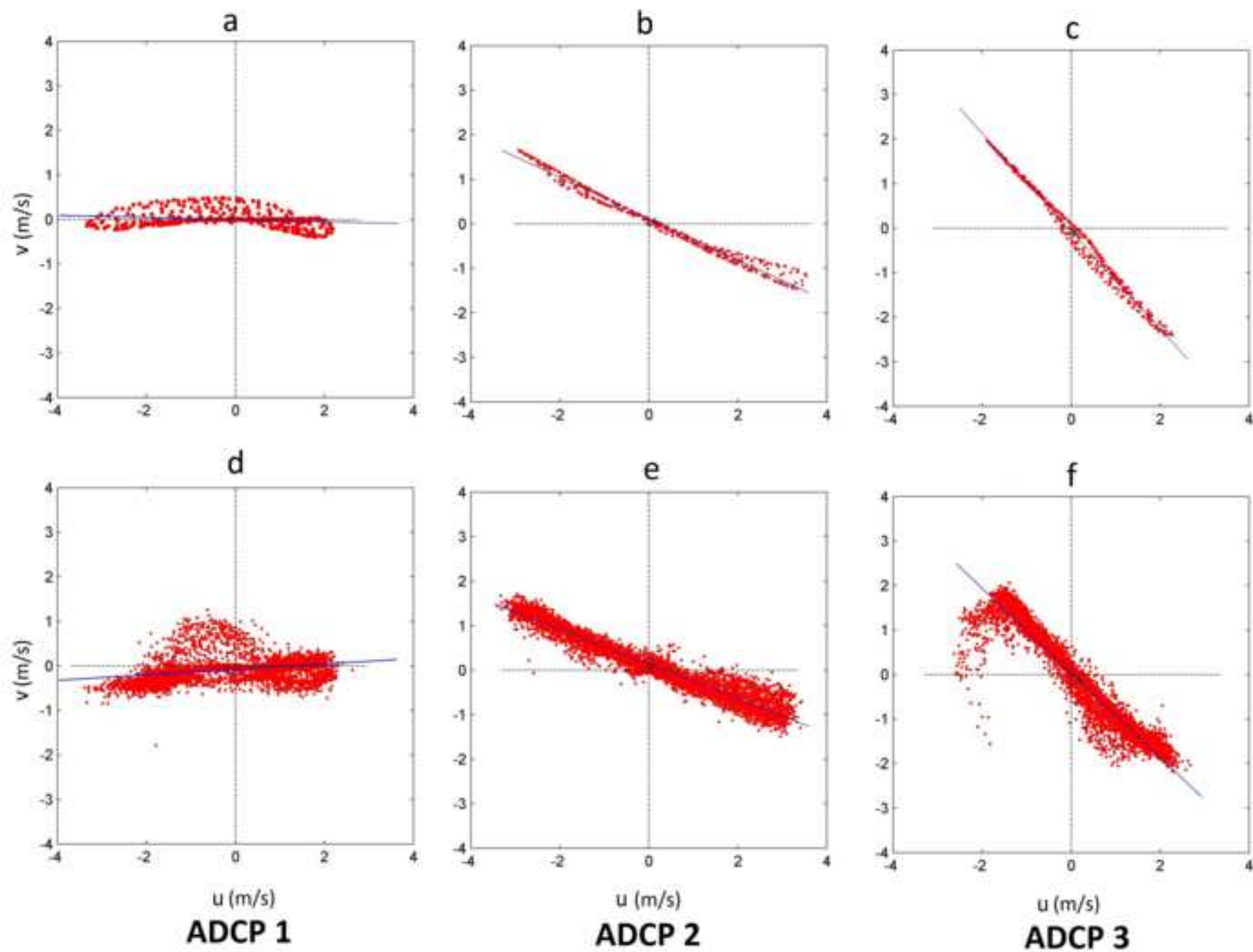
Figure



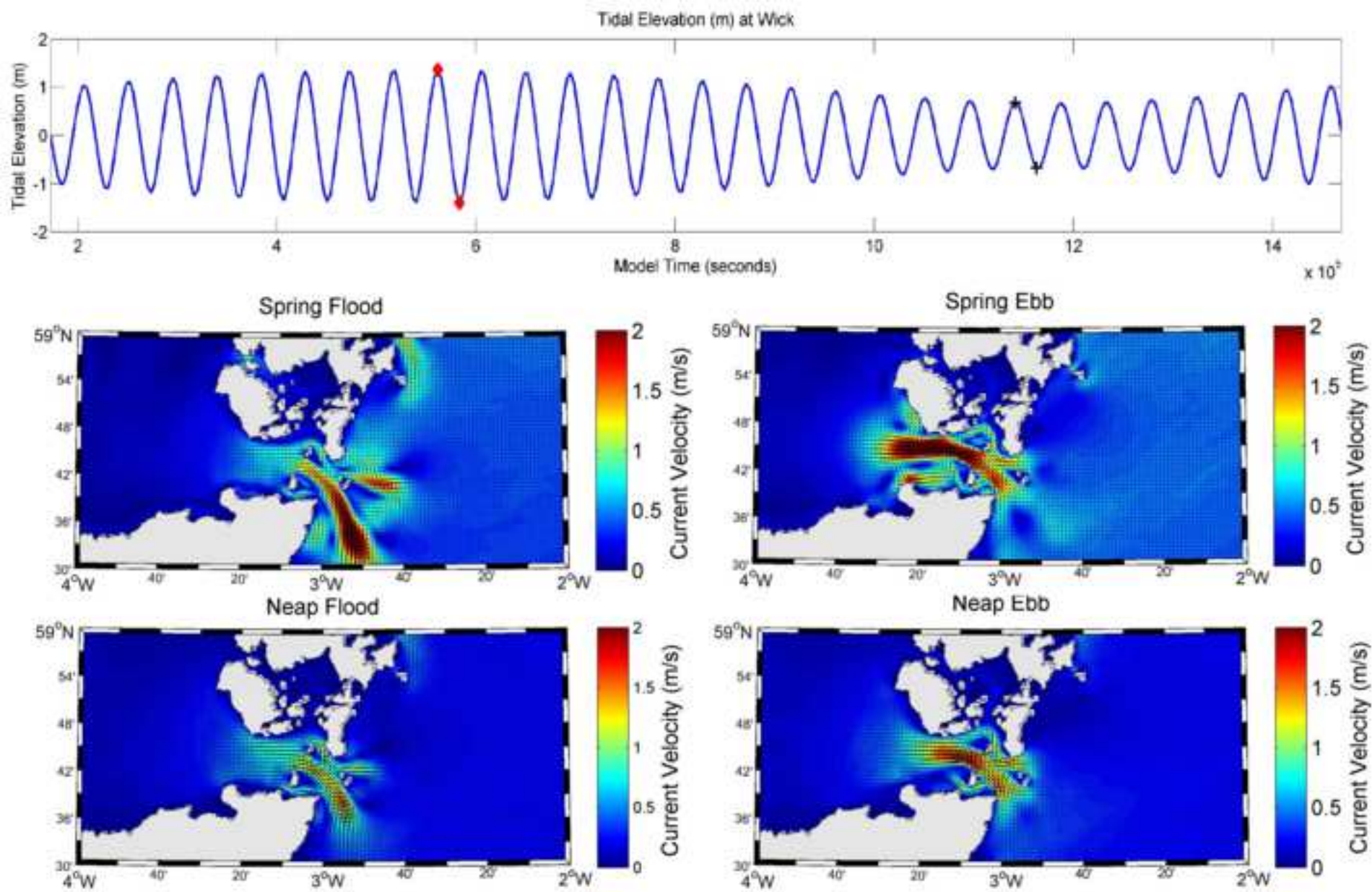




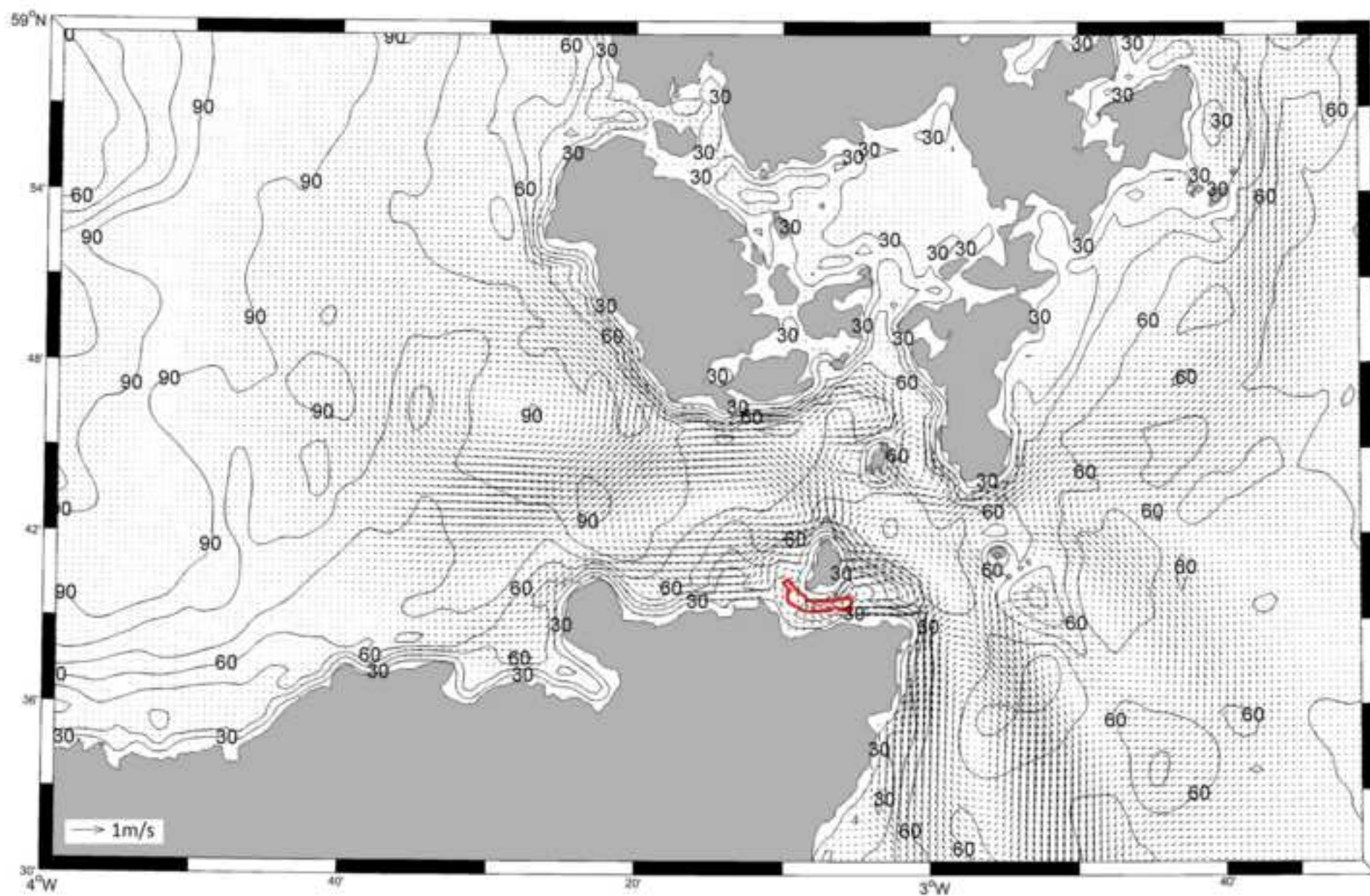
Figure



Figure

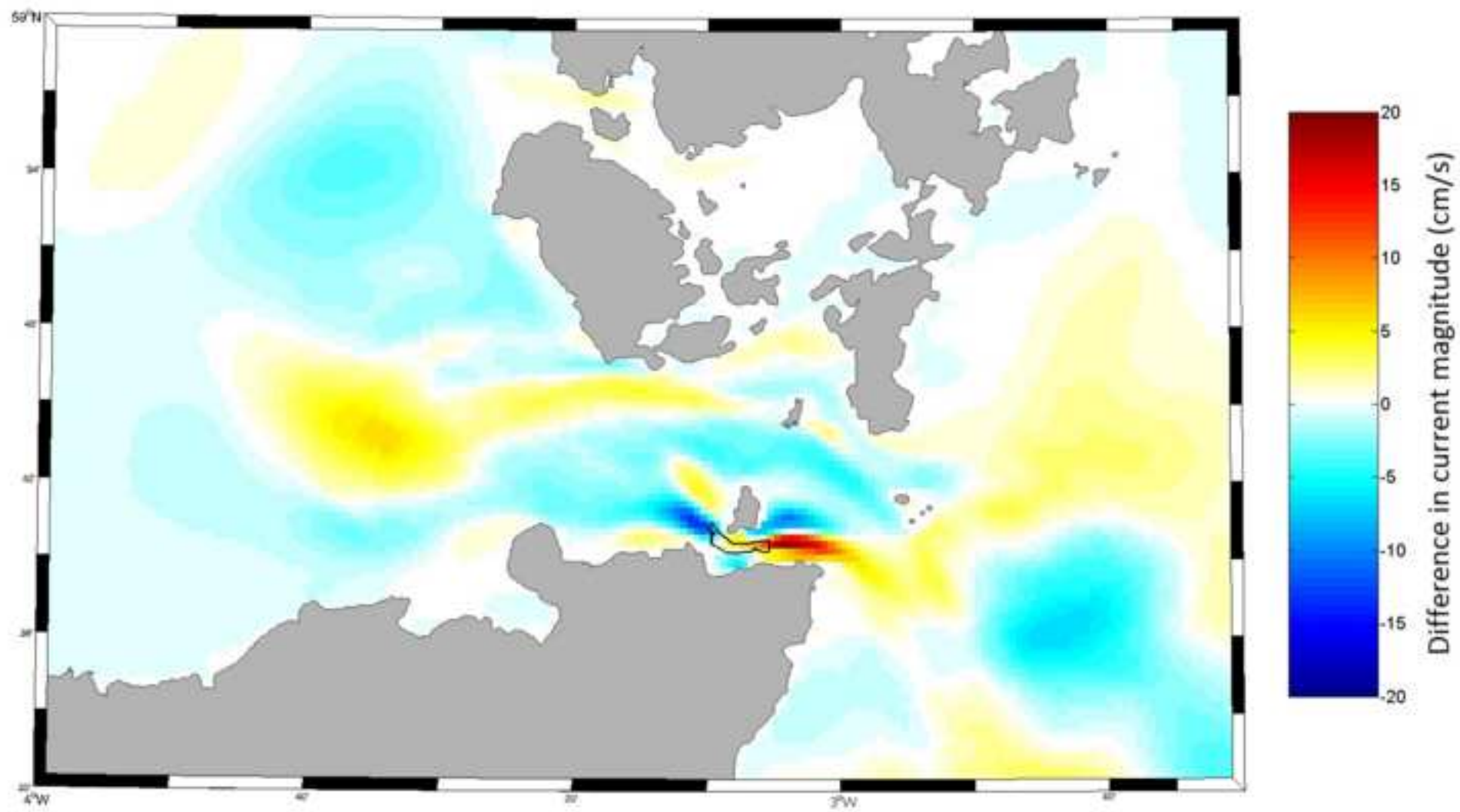


Figure

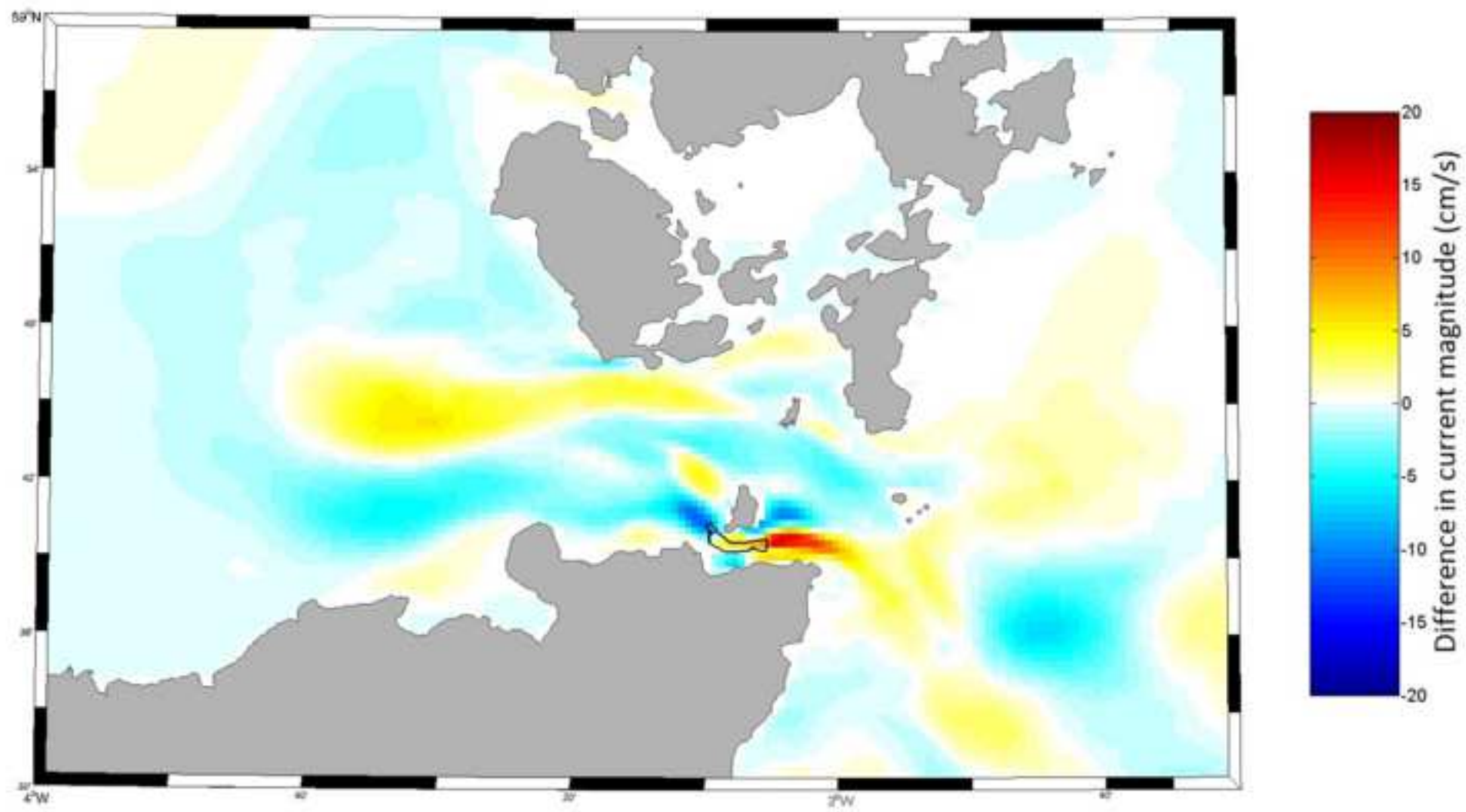




Figure

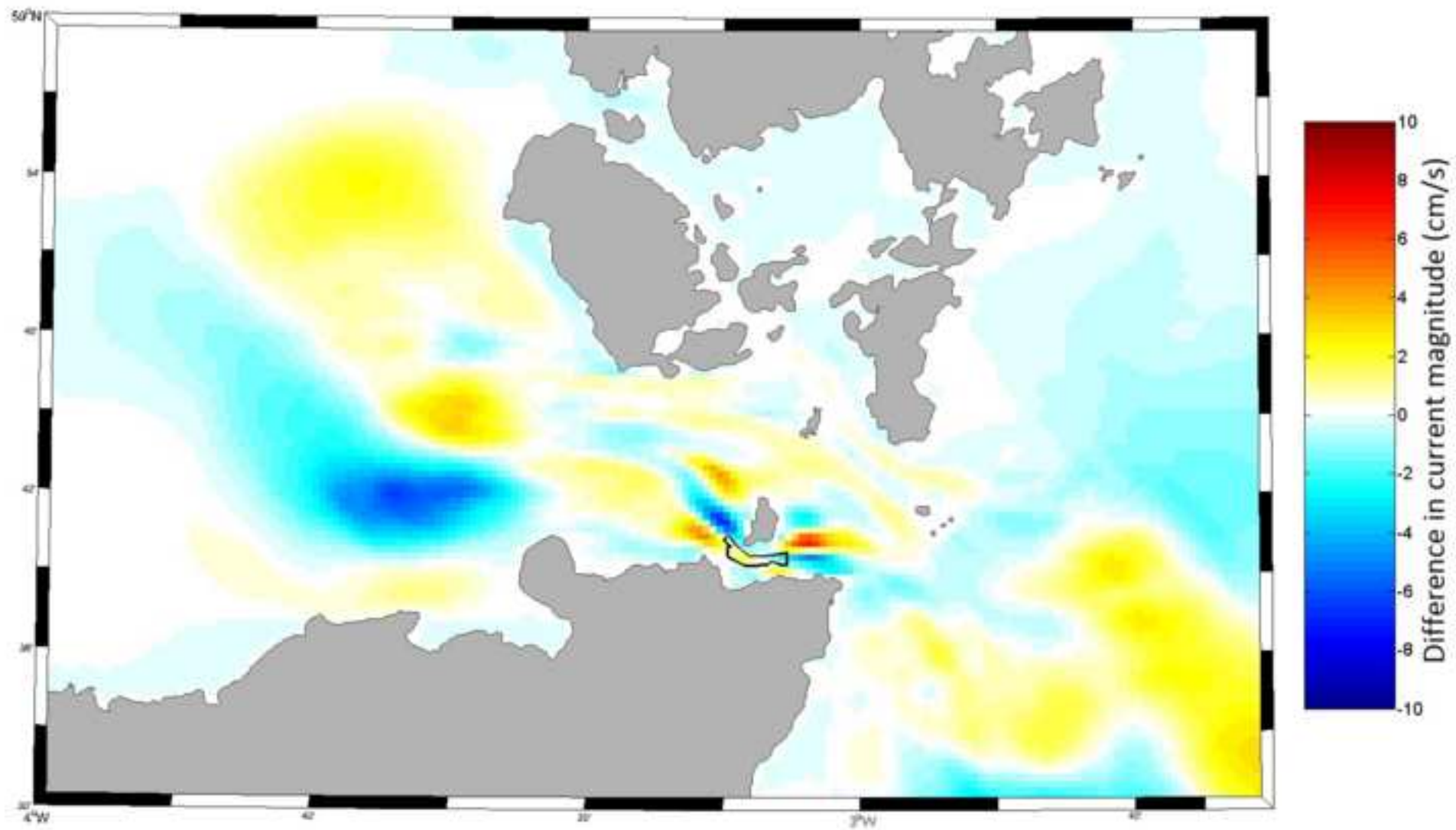


Figure

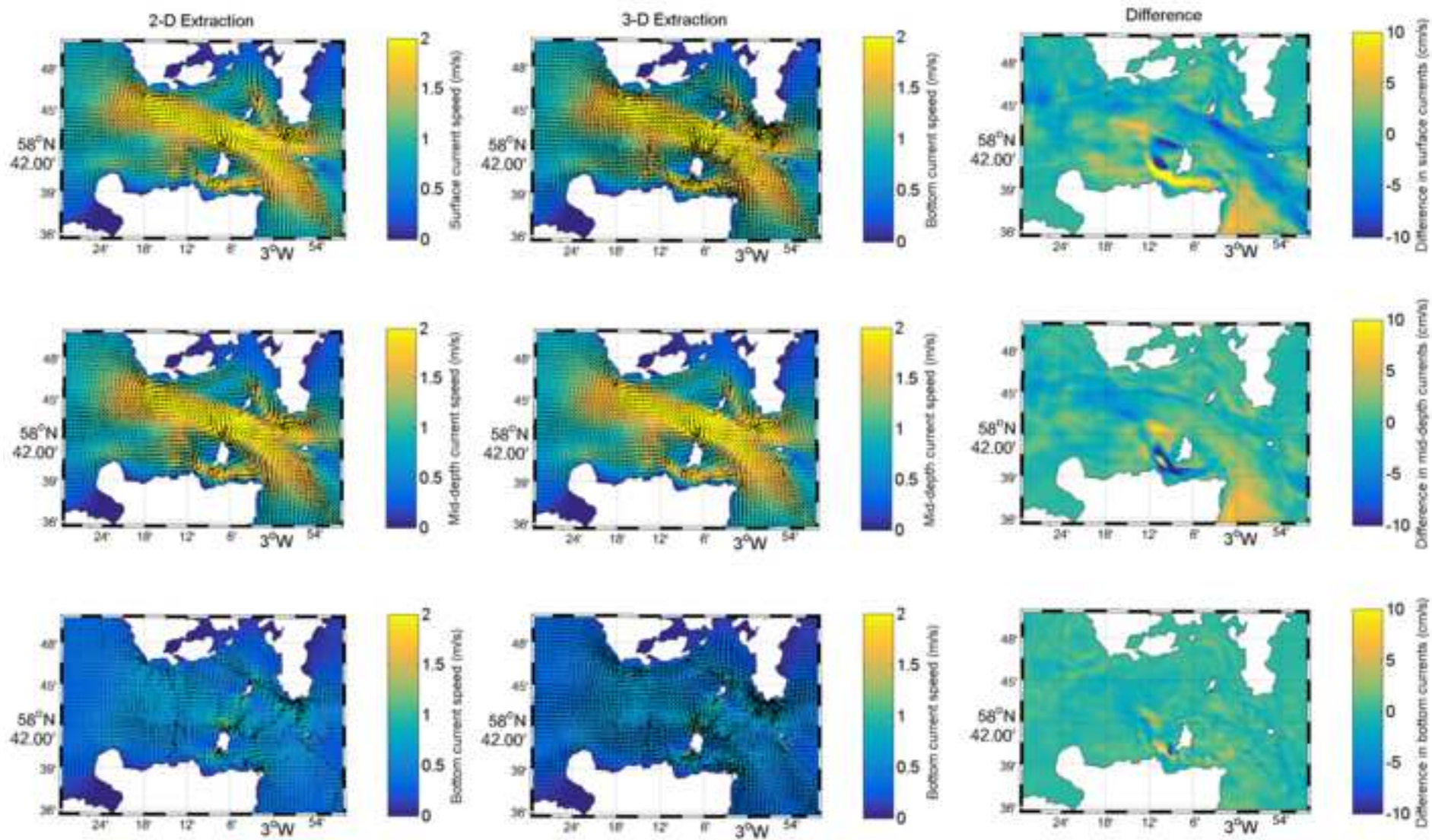




Figure

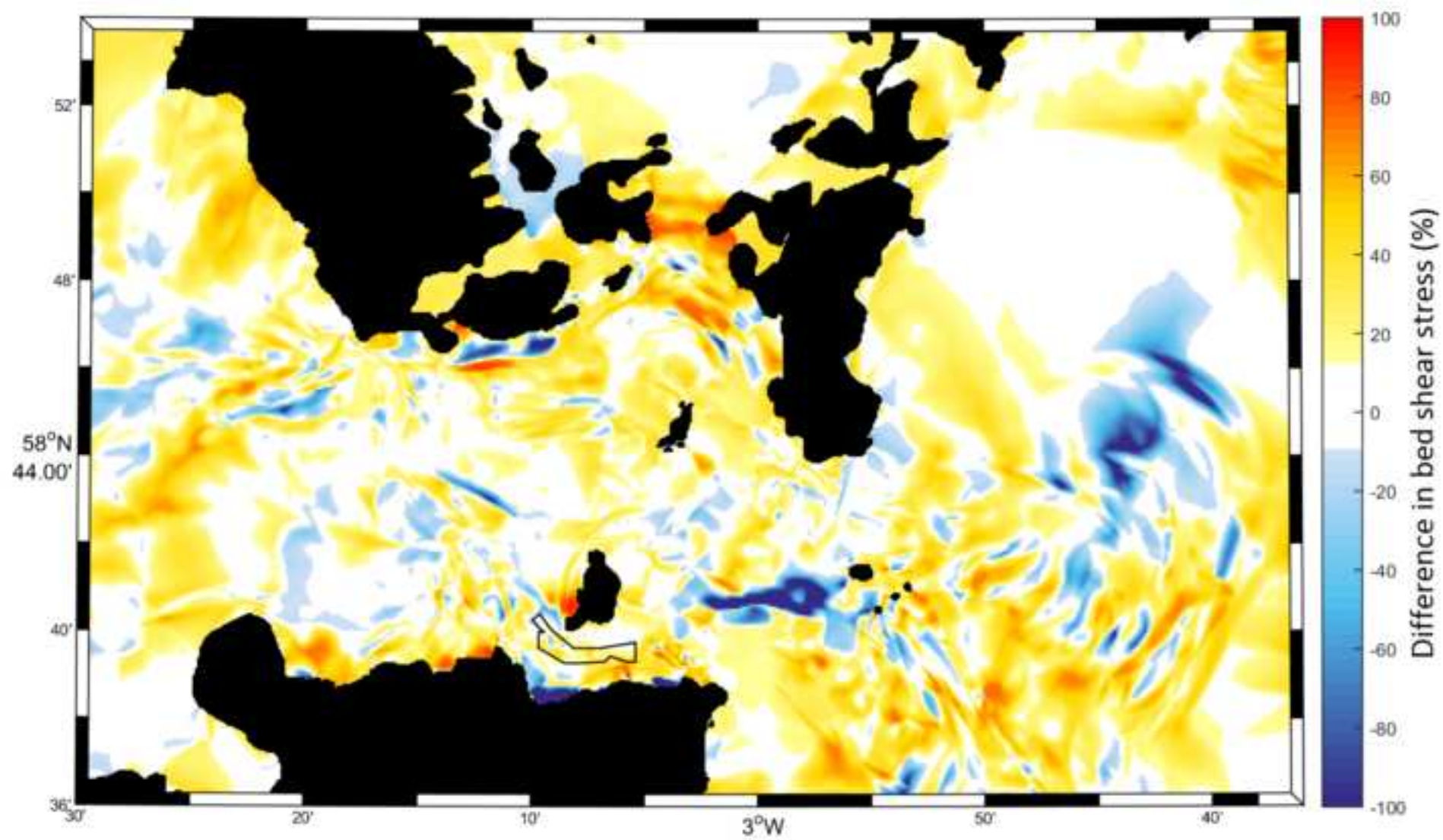


Figure





Figure



## Highlights

- \* We implement 2-D and 3-D tidal energy extraction in a regional ocean model
- \* 2-D tidal energy extraction in models does not capture turbine flow bypass
- \* Simulating 3-D extraction reduces uncertainty in resource and impact assessments